Alma Mater Studiorum - University of Bologna

School of Engineering and Architecture

Department of Industrial Engineering
Second-cycle Degree in Mechanical Engineering

Master degree thesis

in

Modeling and Control of Internal Combustion Engines
and Hybrid Propulsion Systems

Development of a Predictive Control Function for a Plug-in Hybrid Electric Vehicle with Electrically-heated Catalyst

Candidate
Stella Canè

Advisor
Ch.mo Prof. Nicolò Cavina

Co-Advisors
Ing. Lorenzo Brunelli
Ing. Alessandro Capancioni
Ing. Alessandro Perazzo
Ing. Mauro Scassa
Prof. Davide Moro
Prof. Enrico Corti

Academic Year 2020-2021
Session II

Alma Mater Studiorum - Università di Bologna

Scuola di Ingegneria e Architettura

Dipartimento di Ingegneria Industriale
Corso di Laurea Magistrale in Ingegneria Meccanica

Tesi di laurea

in

Motori a Combustione Interna e Propulsori Ibridi

Sviluppo di una funzione di controllo predittiva per un veicolo ibrido elettrico plug-in con catalizzatore riscaldato elettricamente

Candidato
Stella Canè

Relatore
Ch.mo Prof. Nicolò Cavina

Correlatori
Ing. Lorenzo Brunelli
Ing. Alessandro Capancioni
Ing. Alessandro Perazzo
Ing. Mauro Scassa
Prof. Davide Moro
Prof. Enrico Corti

Academic Year 2020-2021
Session II

A mio padre, mia madre e tutti quelli
che mi hanno accompagnato
lungo questo cammino

There are no traffic jams
along the extra mile.

[Roger Staubach]

Abstract

In response to the tightening of European regulations on carbon dioxide (CO_2) and pollutant emissions, in the last years an important evolution of powertrain layout and related control strategies has taken place. New technologies have been developed to improve internal combustion engines efficiency, while more complex exhaust aftertreatment systems (EATS) have become mandatory to be compliant with the tightened pollutant emissions targets, with particular focus on nitrogen oxides (NO_x). The incoming EURO 7 regulation will introduce even more challenging limits, together with a more demanding test procedure focused on real driving scenarios, thus forcing internal combustion engines to be efficient and clean in almost all possible operating conditions. Therefore, an optimized EATS thermal management will be a key point to reach this target, ensuring high pollutants conversion efficiencies and thus reduced tailpipe emissions. Besides the conventional heating strategies based on engine calibration, alternative technologies have been considered in order to speed-up EATS heating phase without affecting engine performance. In particular, a valid solution is represented by electrically heated catalysts (EHCs), which in recent years have become more interesting considering the increasing electrification trend followed by the transport sector in response to CO_2 emission targets. In addition, the increasing amount of data available from vehicle connectivity would allow to fully take advantage of the extreme flexibility of electric hybrid powertrains coupled with advanced EATSs, enabling the development of predictive control strategies aimed to the best trade-off in terms of fuel consumption and pollutant emissions.

In this context, the present activity is focused on the development of a predictive EHC control function for a diesel plug-in hybrid electric vehicle (PHEV) equipped with a EURO 7 compliant EATS, showing the advantages provided by the implementation of a predictive control strategy with respect to a rule-based one. A

preliminary step will be the definition of an accurate powertrain and EATS physical model, starting from already existing and validated applications. Then, a rule-based control strategy managing the torque split between the electric motor (EM) and the internal combustion engine (ICE) will be developed and calibrated, with the main target of limiting tailpipe NO_x emission by taking into account EM and ICE operating conditions together with EATS conversion efficiency. The information available from vehicle connectivity will be used to reconstruct the future driving scenario, also referred to as electronic horizon (eHorizon), and in particular to predict ICE first start. Based on this knowledge, an EATS pre-heating phase can be planned to avoid low pollutant conversion efficiencies, thus preventing high NO_x emission due to engine cold start. Consequently, the final NO_x emission over the complete driving cycle will be strongly reduced with respect to the case in which a rule-based EHC strategy is applied, allowing to comply with the limits potentially set by EURO 7 regulation. Moreover, given the same NO_x emission target, the gain achieved thanks to the implementation of an EHC predictive control function will allow to consider a simplified EATS layout, thus reducing the related manufacturing cost.

The promising results achieved in terms of NO_x emission reduction show the effectiveness of the application of a predictive control strategy focused on EATS thermal management and highlight the potential of a complete integration and parallel development of involved vehicle physical systems, control software and connectivity data management.

Abstract in lingua italiana

In risposta all'inasprimento delle normative europee riguardanti le emissioni di inquinanti e anidride carbonica (CO_2), negli ultimi anni si è assistito ad un'importante evoluzione del settore dei trasporti, sia a livello di architettura del powertrain che delle relative strategie di controllo. Nuove tecnologie sono state sviluppate al fine di migliorare l'efficienza dei motori a combustione interna, mentre sistemi di post-trattamento dei gas di scarico sempre più complessi sono diventati indispensabili per rispettare i limiti sulle emissioni di inquinanti, con particolare riferimento agli ossidi di azoto (NO_x). La nuova normativa EURO 7 in arrivo introdurrà limiti ancora più stringenti, insieme ad una procedura di omologazione più impegnativa focalizzata su scenari di guida reale, obbligando quindi i motori a combustione interna ad essere efficienti e "puliti" in praticamente tutte le possibili condizioni operative. Pertanto, una gestione termica ottimale del sistema di post-trattamento sarà un punto chiave per raggiungere questo obiettivo, assicurando alte efficienze di conversione delle specie inquinanti e di conseguenza ridotte emissioni allo scarico. Oltre alle strategie convenzionali basate sulla calibrazione del motore, sono state prese in considerazione tecnologie alternative per velocizzare la fase di riscaldamento del sistema di post-trattamento che allo stesso tempo non penalizzino le performance del motore. In particolare, una valida soluzione è rappresentata dai catalizzatori riscaldati elettricamente (electrically-heated catalysts, EHCs), una soluzione che negli ultimi anni è diventata interessante considerando l'attuale trend verso un'elettrificazione sempre più spinta del settore dei trasporti, in risposta ai limiti sempre più stringenti sulle emissioni di CO_2. Inotre, la quantità crescente di dati resi disponibili dalla connettività dei veicoli, permetterebbe di sfruttare pienamente l'estrema flessibilità dei powertrain ibridi abbinati con sistemi di post-trattamento avanzati, rendendo possibile lo sviluppo di strategie di controllo predittive finalizzate a raggiungere il miglior

compromesso in termini di consumo di combustibile ed emissioni di inquinanti.

In questo contesto, la presente attività si focalizza sullo sviluppo di una funzione predittiva per il controllo di un EHC su un veicolo ibrido plug-in dotato di un sistema di post-trattamento in linea con gli standard EURO 7, con il fine di mostrare i vantaggi introdotti dall'implementazione di una strategia di tipo predittivo rispetto ad una di tipo rule-based. Un passo preliminare consisterà nel definire un modello fisico accurato che sia rappresentativo del powertrain e del sistema di post-trattamento considerati, a partire da applicazioni già esistenti e precedentemente validate. A seguire, sarà sviluppata una strategia di controllo di tipo rule-based per gestire la divisione di coppia tra motore elettrico e termico, che verrà poi calibrata con l'obiettivo di minimizzarre l'emissione di NO_x, tenendo in considerazione sia le condizioni operative dei due motori che l'efficienza di conversione del sistema di post-trattamento. Le informazioni disponibili grazie alla connettività verranno quindi utilizzate per ricostruire il futuro scenario di guida, indicato anche come electronic horizon (eHorizon), e in particolare per predire la prima accensione del motore termico. In base a questa informazione, si può pianificare una strategia di preriscaldo del sistema di post-trattamento per evitare basse efficienze di conversione, prevenendo così l'elevato livello di emissioni di NO_x a seguito dell'accensione a freddo del motore. Di conseguenza, le emissioni registrate sull'intero ciclo di guida risulteranno decisamente ridotte rispetto al caso in cui venga applicata una strategia rule-based, permettendo di rispettare i limiti potenzialmente introdotti dalla normativa EURO 7. Inoltre, fissato lo stesso obiettivo in termini di emissioni di NO_x, il miglioramento introdotto grazie all'implementazione di una funzione di controllo predittiva per l'EHC permetterà di prendere in considerazione una semplificazione del layout del sistema di post-trattamento, riducendo di conseguenza i costi relativi alla produzione dei componenti.

I risultati promettenti raggiunti in termini di riduzione delle emissioni di NO_x mostrano l'efficacia dell'applicazione di una strategia di controllo predittiva incentrata sulla gestione termica del sistema di post-trattamento e mette in luce il potenziale di una completa integrazione e sviluppo in parallelo dei sistemi fisici coinvolti, del software di controllo e della gestione dei dati di connettività del veicolo.

Acknowledgments

Vorrei ringraziare in primo luogo il Professor Nicolò Cavina, che grazie alla passione e dedizione per il suo lavoro mi ha fatto avvicinare a quest'ambito di ricerca e mi ha dato la concreta opportunità di svolgere questa attività di tesi. Un ringraziamento speciale a Lorenzo, che mi ha affiancato durante tutto questo percorso e che, con la sua pazienza e simpatia, ha saputo fornirmi sempre il giusto supporto tecnico e morale. Vorrei inoltre ringraziare Capa, Alessandro P. e Mauro per i loro consigli, la loro professionalità e disponibilità, insieme a tutti i membri del team di FEV Bologna che hanno preso parte alla realizzazione di questo elaborato. Infine ringrazio tutte le persone che ho avuto modo di conoscere in questi mesi e che a loro modo hanno contribuito a rendere questo percorso un'esperienza da ricordare.

Contents

List of figures

List of tables

Nomenclature

Acronyms

$BSNO_x$	Brake Specific NO_x (emission)
AC	Alternate Current
ADAS	Advanced Driver Assistance System
BEV	Battery Electric Vehicle
BMEP	Brake Mean Effective Pressure
BSFC	Brake Specific Fuel Consumption
BSG	Belt-driven Starter Generator
CD	Charge-Depleting
CS	Charge-Sustaining
DC	Direct Current
DOC	Diesel Oxidizing Catalyst
DoE	Design of Experiments
DPF	Diesel Particulate Filter
EATS	Exhaust After-Treatment System
ECU	Engine Control Unit
EHC	Electrically-Heated Catalyst
EM	Electric Motor
EV	Electric Vehicle
GHG	Green-House Gas
HC	HydroCarbon(s)
HCU	Hybrid Control Unit
HEV	Hybrid Electric Vehicle
HTC	Heat Transfer Coefficient

HV	High-Voltage
ICE	Internal Combustion Engine
ISG	Integrated Starter Generator
LCV	Light Commercial Vehicle
LPS	Load-Point Shift
LV	Low-Voltage
MiL	Model-in-the-Loop
NEDC	New European Drive Cycle
PGM	Platinum-Group Metal
PHEV	Plug-in Hybrid Electric Vehicle
PI	Proportional-Integral (controller)
PM	Particulate Matter
PS	Predictive Strategy
RBS	Rule-Based Strategy
RDE	Real-Driving Emissions (test)
SCR	Selective Catalytic Reduction
SiL	Model-in-the-Loop
SoC	State of Charge
V2C	Vehicle-To-Cloud
V2I	Vehicle-To-Infrastructure
V2P	Vehicle-To-Pedestrian
V2V	Vehicle-To-Vehicle
V2X	Vehicle-To-Everything
WLTC	Worldwide harmonized Light vehicles Test Cycle
WLTP	Worldwide harmonized Light vehicles Test Procedure

Chapter 1

Introduction

1.1 Motivations, challenges and targets

In the last decades, the growing level of industrialization and urbanization in several developing countries has led to a significant increase in the global atmospheric concentration of anthropogenic greenhouse gases. As is known, this is directly connected to the main concerns of global warming and climate change, causing environmental degradation and many severe implications that the world is already facing. In this context, researchers have pointed out that the four main greenhouse gases which should attract serious global attention today are carbon dioxide (CO_2), methane (CH_4), nitrous oxide (N_2O) and sulfur dioxide (SO_2). More in detail, although water vapor is the most abundant greenhouse gas naturally present in the atmosphere, CO_2 is the most emitted one [1]; in addition, recent studies have highlighted that the transport sector gives a relevant contribution to the emission of greenhouse gases, being responsible for 16.2% of the CO_2 overall emission [1][2].

With regard to pollutant emissions, following the evolution of combustion processes and aftertreatment technologies over the last years, today the attention is mainly focused on the issue related to nitrogen oxides, a group of highly reactive gaseous compounds containing nitrogen and oxygen in different proportions. Among these, the aforementioned N_2O is a strong greenhouse gas, with a global warming potential (GWP) approximately 300 times higher with respect to the one of CO_2. On the other hand, NO_x (as the sum of NO and NO_2 is commonly referred to) has direct

Figure 1.1: Annual CO_2 emissions by world region [2].

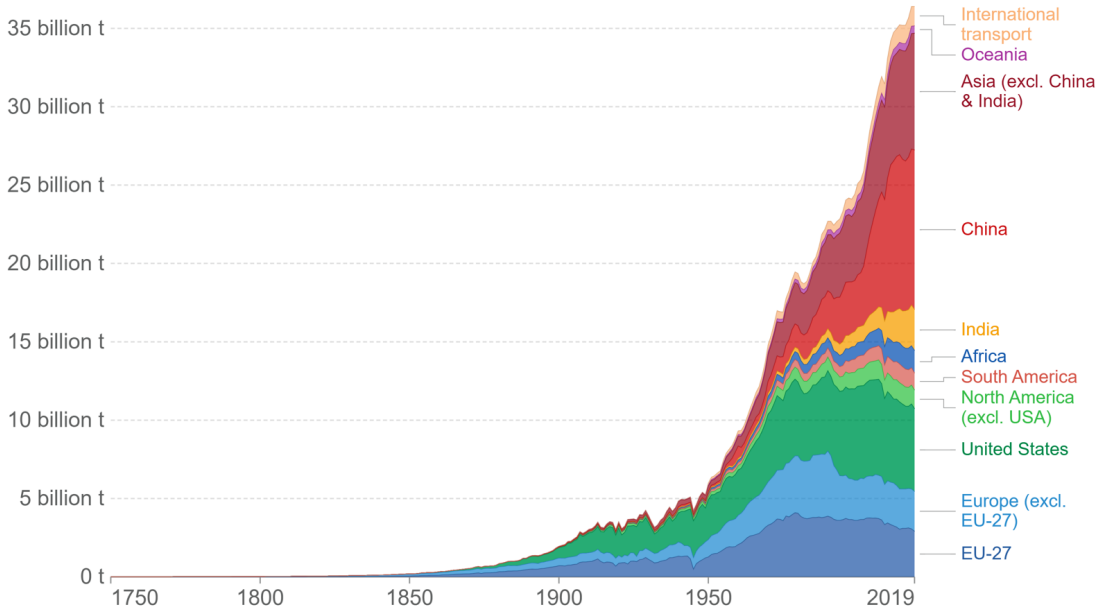

effects on human health as well as on the environment; some examples are protein oxidation, cell membrane damage, alteration of the immune system, green leaves ageing, and reduction of photosynthetic activity and biomass production [3][4]. According to [5], the road transport sector is one of the main sources of NO_x emissions in Europe (39% in 2017), which combined to the relevant contribute to the CO_2 overall emission, makes it clear the need for a greener and smarter mobility.

In response to this need, in recent years European regulation on CO_2 and pollutant emissions has become increasingly strict for almost the entire vehicle fleet, covering transport classes that go from passenger cars to heavy-duty applications. Looking to the next decade, the European Council has set a 15% reduction target on CO_2 emission from 2025 with respect to 2021 standards for the entire new vehicle fleet, and up to 31% and 37.5% reduction from 2030 for heavy-duty vehicles and passenger cars fleet respectively [6]. Of course, these demanding requirements in terms of internal combustion engines efficiency must meet at the same time increasingly stringent limitations regarding pollutant emissions, with a particular focus on

Figure 1.2: Global greenhouse gases emissions by sector measured in tonnes of carbon dioxide-equivalents CO_{2eq} [2].

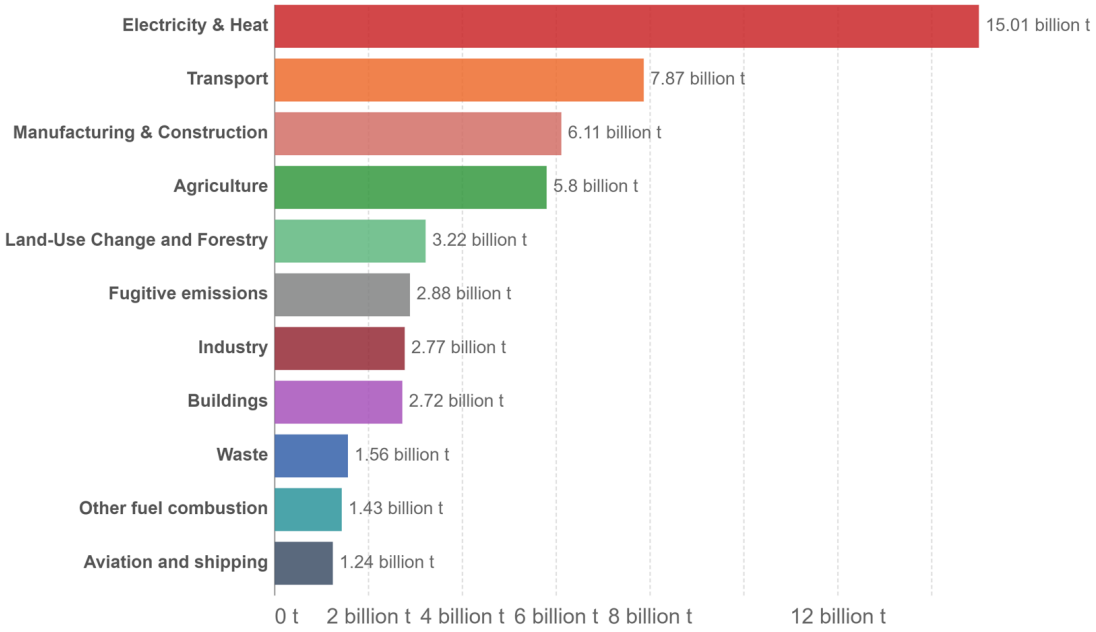

NO_x emissions. [7]. Reaching these targets is even more challenging since homologation driving cycles are required to be more representative of real driving conditions, leading to the introduction of real driving cycles (RDE) beside the standard WLTP laboratory test procedure, forcing internal combustion engines to be more efficient and cleaner than before and in a wider range of operating conditions [8]. To date, the tightening of emissions targets has been one of the main driving factors for the improvement and development of new powertrain and aftertreatment technologies. Diesel engines, which are by nature more efficient, have been facing the main concern related to NO_x and PM emissions, leading to the evolution of high-pressure injection systems, of combustion chamber design and of aftertreatment system layout. On the other hand, gasoline engines evolved following higher efficiency targets, with the introduction of technologies like variable valve actuation, exhaust gas recirculation, direct fuel injection and lean-burn, aimed to reduce pumping losses and increase thermodynamic efficiency. Nevertheless, this evolution makes gasoline engines move

towards typical diesel engine design solutions, as high compression ratio, direct injection and lean combustion, with all the related pollutants problems, thus making mandatory the parallel development of an advanced exhaust aftertreatment system (EATS) for both gasoline and diesel engines to meet efficiency and pollutant targets at the same time.

1.2 Overview: hybrid electric vehicles and connectivity

As widely seen in recent years, an effective way to reduce fuel consumption and keep CO_2 emissions below the limits is to introduce an electric machine (EM) to support the internal combustion engine (ICE) in the less efficient operating points. Since two power sources are employed to fulfil driver torque demand, hybridization introduces additional degrees of freedom concerning torque split and on-board energy management, making it necessary to develop more complex control strategies. On the other hand, despite the growing complexity during calibration phase, the developed control strategies can be used to take advantage of the flexibility of these systems, aiming to follow different targets in terms of brake specific fuel consumption (BSFC), raw NO_x emissions and exhaust gas temperature, depending on engine operating conditions, EATS conversion efficiency and battery state of charge (SOC).

More in detail, hybrid electric vehicles (HEVs) can be divided into three categories based on powertrain layout and on how power is transferred to the wheels:

- **Series topology** The wheels are directly driven by an EM powered by a battery storage system, while the ICE is used as an auxiliary power unit only to charge the battery in case of need;
- **Parallel topology** Both the ICE and the EM(s) can directly provide torque to the wheels thanks to a proper arrangement of gearbox and clutches;
- **Power-split topology** Both series and parallel working modes can be applied.

With particular reference to HEVs parallel topology, several architectures based on EM(s) position within the driveline are possible (Fig. 1.3):

- **P0** The motor is coupled to the engine by mean of a belt. In this case, the EM is called BSG (Belt-driven Starter Generator);
- **P1** The motor/generator is directly mounted on the crankshaft upstream of the clutch. The EM is called ISG (integrated Starter Generator);
- **P2** The EM is decoupled from the ICE by a clutch allowing pure electric drive;
- **P3** The EM is mounted on the secondary shaft of the gearbox;
- **P4** The EM is directly mounted on the front or rear axle.

Figure 1.3: Schematic representation of parallel hybrid powertrain architectures

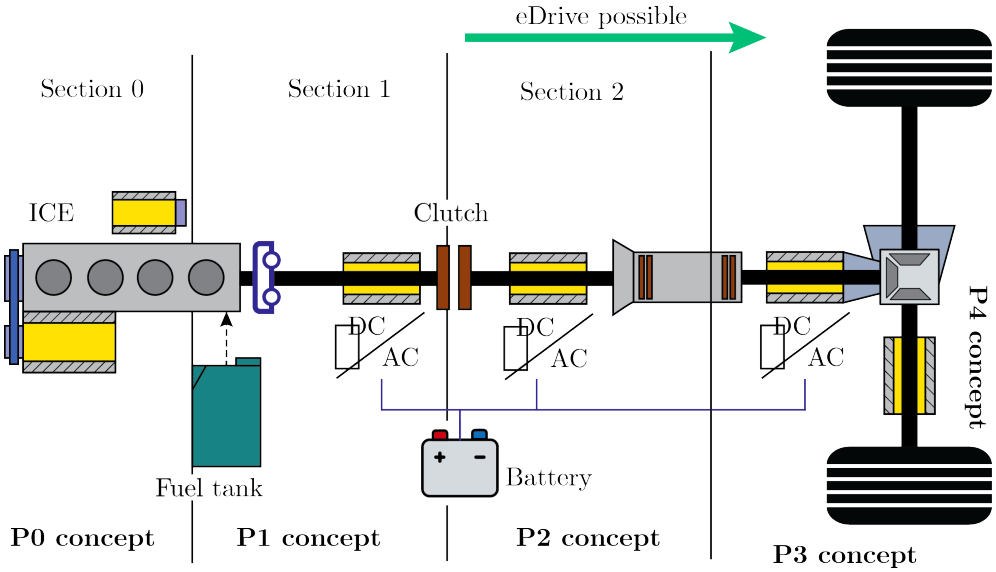

Moreover, HEVs currently available on the market can be classified according to different levels of hybridization, depending on the size of the battery and of the electric machine:

- **Micro Hybrid** It is the lowest level of hybridization, with a 12 V battery storage capacity that is slightly higher with respect to the one installed on conventional vehicles, allowing to perform Start and Stop and other additional functionalities;

- **MHEV (Mild or Medium HEV)** A compact EM is used to provide limited driving support to the engine, as stop/start features and extra power assist during significant acceleration phases. It can also work as a generator during deceleration phases allowing regenerative braking. An additional low voltage battery system (48 V) enables the actuation of energy management strategies providing a minimum range of electric drive;

- **FHEV (Full HEV)** The increased size of the electric machines and batteries allows a significant range of full electric drive, enabling the development of more complex and efficient energy management strategies. As for MHEVs, off-vehicle charging is not possible, so battery recharging can only happen through braking recuperation or engine operation;

- **PHEV (Plug-in HEV)** It is the highest degree of hybridization. As for FHEVs, large batteries ensure an extended all-electric range, with the additional possibility of external battery charging by connecting the vehicle to the power grid. Of course the idea is to minimize on-road emission by avoiding ICE operation as much as possible.

With particular reference to the highest levels of hybridization, which means FHEVs or PHEV, significant advantage in terms of fuel consumption and pollutant emissions can be taken thanks to the high flexibility of these systems. Moreover, innovative technologies are being implemented both on the vehicle and the infrastructure, such as wireless communication, cloud computing, innovative sensors, and artificial intelligence functions (as computer vision). These technologies result in advancements in the vehicle-to-everything (V2X) communication industry, including vehicle-to-vehicle (V2V), vehicle-to-infrastructure (V2I), and vehicle-to-network (V2N) communication. Together with the latest Advanced Driver-Assistance Systems (ADAS), all the mentioned technologies allow calculating an electronic horizon (shortly known as eHorizon) which represents a virtual reconstruction of the trip ahead for a planned route. It is conventionally divided into "short horizon", which comprehends information about nearby vehicles and traffic lights, and the "long horizon", which includes information about selected route, slope, legal speed limits and static stop events. Such information can be used to manage the available energy

more efficiently and sustainably, as it allows the development of predictive control strategies aimed to find the best trade-off between efficiency and raw emission control, as widely evidenced by the literature [9][10]. In addition, as deeper underlined in the next section, engine light-off and vehicle speed profile prediction can be used also for the smart management of the EATS, allowing to search for the best solution in terms of energy and fuel consumption that prevents low pollutant conversion efficiencies.

1.3 State of the art: EATS thermal management

Nowadays, evolved aftertreatment technologies, including diesel oxidation catalyst (DOC), lean NO_x trap (LNT) and selective catalytic reduction (SCR) are valid solutions to limit tailpipe pollutant emissions and meet the targets imposed by the regulations for both diesel and gasoline lean-burn engines. However, despite the unquestioned gain achieved in terms of pollutant emission reduction, additional efforts are required in terms of systems complexity and costs deriving from the issues related to these types of combustion, as already mentioned [11][12]. Conversion efficiency can be very high provided the proper operating temperature range. In fact, the most critical situation is the one related to cold operation of the catalytic converter during engine start and warm-up, and so lower conversion efficiency, being more relevant for diesel engines rather than gasoline engines due to lower exhaust gas temperature. This issue involves both conventional and hybrid electric vehicles, being even more relevant for the latter, due to repeated engine starts and stops and reduced engine load thanks to electric motor torque assist, which may reduce substantially the temperature of the EATS. Moreover, another critical situation that may occur in HEVs is the so-called ICE high-power cold start, namely when the engine is forced to start to support the EM in case of a high torque request. In this situation the engine must go from an off-state to a high-speed and load-state as fast as possible to fulfil the driver demand, and since it could happen after an extended e-drive phase, the EATS temperature can be very low, thus strongly affecting the resulting pollutant emission ([13]). Therefore, many technologies and strategies have been developed trying to solve this problem, including methods based on engine calibration, torque split management and EATS layout [14]. Start of combustion delay,

both for diesel and gasoline engines, can be very effective to reduce catalyst light-off time; however, it leads to significant fuel penalty, which imposes limitations for its application. Higher idle speed provides a higher exhaust gas flow rate, speeding up the catalyst heating phase; however, it is not sufficient as itself and it also implies higher fuel consumption. A valid alternative that can be applied to HEVs is given by the request of a higher load to the engine, using the additional power to recharge the battery. Wastegate valve control, variable nozzle and variable geometry turbines can bring advantages in terms of exhaust gas temperature increase by reducing gas expansion and related temperature drop; however, all these methods affect also engine performance, causing a reduction of available engine power during cold start. So, in summary, thermal management methods based on engine calibration show a limited potential due to their significant fuel penalty and performance degradation, but they do not require the installation of any additional device, which is actually a significant advantage. On the other hand, acting on EATS layout, the installation of after-burners or reformers, coupled with secondary air introduction in the first case, allows to strongly speed-up catalyst heating phase. Even if these methods are very effective and do not affect engine operation, they imply important fuel penalties and significant additional costs. Thermal insulating and heat storage materials have been applied to keep catalyst at high temperature for a longer time, however, they need special materials that can face such demanding conditions and they are suitable just for vehicles running regularly and for very long periods.

In this context, according to the state of the art, electrically heated catalysts (EHCs), employing one or more discs upstream the catalyst that are heated by current flowing in high-resistance circuits, provide an effective solution to reduce emissions during engine cold start without affecting engine performance, since they act directly on the exhaust line [15][16][13]. Of course, this heating method needs the installation of an additional device and the availability of a significant amount of electric energy to power it. However, promising results reached in terms of shortening catalyst light-off time make it deserve further investigation to understand the actual potential of this technology, especially considering the current electrification trend that the transport sector is following in response to CO_2 emission targets, meaning that electrical power needed by the EHC would be already available on

the vehicle with no need for important modifications on hybrid powertrain architecture. With a particular focus on HEVs, the advantages and flexibility introduced by this technology are even clearer if integrated with a predictive control strategy [17][18]. In fact, the knowledge of the future driving path allows predicting engine starts and operating conditions, avoiding low-temperature operation of the EATS while searching for the best trade-off in terms of catalyst conversion efficiency and energy consumption. In parallel, as supported by literature, the same information about future driving conditions could be employed also for the management of other EATS devices, for example by developing smart strategies to optimize particulate filter regeneration or urea consumption of SCR systems [17][19].

From this perspective, the complete integration between hybrid powertrain control, EATS thermal management and vehicle connectivity could be the right solution to be compliant with both CO_2 and pollutant emission future limits. In this context, the focus of this work is the development of an EHC predictive control function for a diesel hybrid light commercial vehicle (LCV) equipped with an advanced EATS, that will allow to be compliant with likely future limits introduced by the incoming EURO7 regulation, solving the main issue related to cold start NO_x emission, that will be unacceptable looking to more stringent incoming limitations.

This master thesis activity has been carried out at Green Mobility Research Laboratory, born by the collaboration between the University of Bologna and FEV Italia s.r.l, internationally recognized leader in design and development of advanced gasoline, diesel and hybrid powertrains and vehicle systems.

Chapter 2

Vehicle model definition

2.1 Vehicle layout definition

2.1.1 Hybrid powertrain

The vehicle selected as a case study for this activity is a P2 Diesel PHEV classified as a light commercial vehicle (LCV). The chosen hybrid architecture, represented in Fig. 2.1, provides high flexibility in terms of possible operating modes and torque split strategies. The location of the EM, thanks to the separation clutch, allows to perform effective regenerative braking as well as pure electric drive. The combination of a 9.4 kWh high-voltage (HV) battery and a 90 kW/440 Nm electric motor ensures a significant all-electric range with a top speed that can reach 130 km/h, depending on hybrid strategy calibration. The electric power unit is paired with a 2.3-litre compression ignition engine and a 6-speed automatic transmission. The main vehicle specifications are listed in Tab. 2.1.

The operating mode between pure-electric drive and hybrid drive is managed through a calibrated strategy based on vehicle speed, requested torque and battery state of charge (SoC). Focusing on hybrid operating mode, different configurations are possible thanks to P2 architecture: the EM can provide additional torque to support the ICE when the driver request is particularly relevant or, on the contrary, it can operate as a generator to charge the battery with the engine providing additional torque with respect to the driver request, allowing to follow the best trade-off between fuel economy and pollutant emissions. A so-called range-extender mode is

Figure 2.1: Schematic representation of vehicle hybrid powertrain architecture.

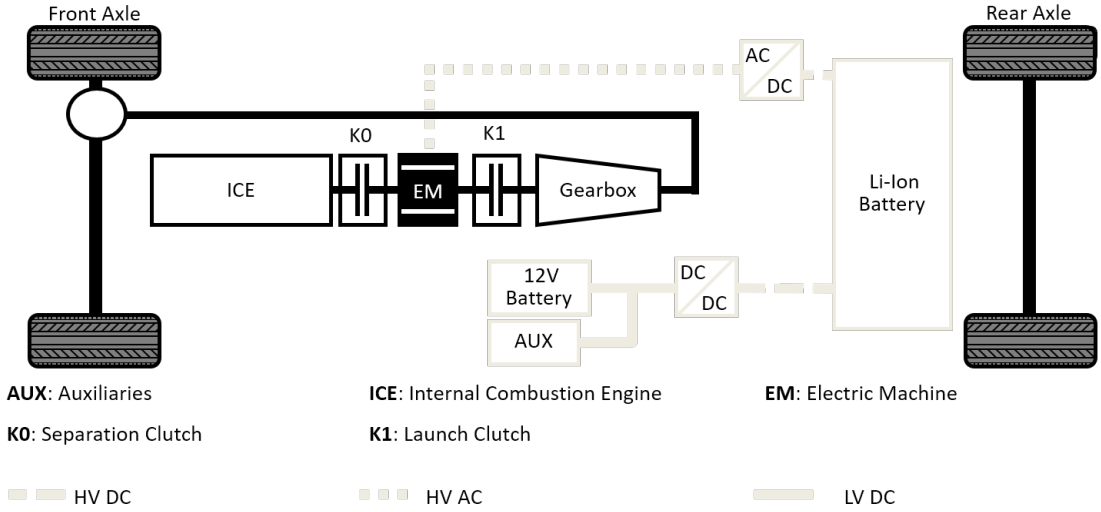

Table 2.1: Main powertrain and vehicle specifications.

Vehicle	Curb weight	2750 kg
	Configuration	P2, front wheel drive
Engine	Type	Turbocharged Diesel
	Displacement	2.3 l
	Rated power	95 kW @ 3000 rpm
	Rated torque	380 Nm @ 2000 rpm
	Gearbox	6-DCT
Electric machine	Type	PM synchronous
	Peak power	90 kW
	Peak/continuous torque	440/260 Nm
	Maximum speed	6000 rpm
Battery	Type	Lithium-ion polymer
	Capacity	9.4 kWh / 25.5 Ah
	Nominal voltage	370 V

also possible when the vehicle is at stand-still and the engine is running for the sole purpose of charging the battery. Hybrid strategy definition and calibration will be deeply discussed in chapter 3.

2.1.2 Exhaust aftertreatment system

As mentioned in chapter 1, an advanced EATS is mandatory to meet the demanding targets imposed by the regulation in terms pollutant emissions, with particular reference to NO_x emissions, without affecting engine efficiency, in order to be compliant with CO_2 emission limits at the same time. Therefore, the modelled vehicle is equipped with a state-of-the-art Diesel EATS, represented in Fig. 2.2, which includes the following devices:

- Electrical heater;
- Diesel Oxidizing Catalyst (DOC);
- Low Thermal Mass Selective Catalytic Reduction (LTM-SCR) catalyst;
- SCR-coated Diesel Particulate Filter (SDPF);
- SCR catalyst.

Figure 2.2: Schematic representation of vehicle EATS architecture.

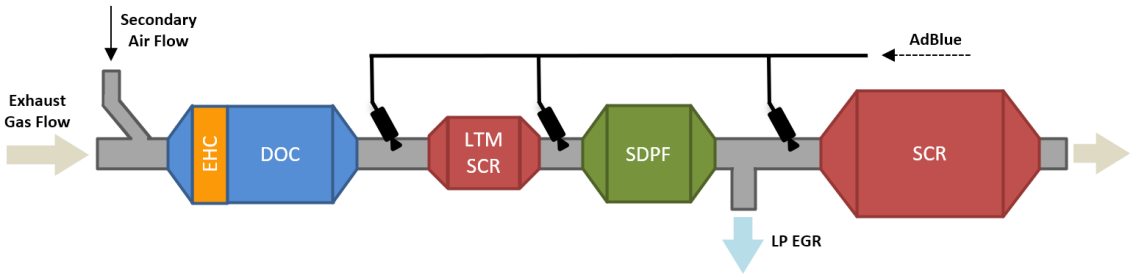

A summary description of the main functions and principles of operation of the mentioned devices is given in the following paragraphs.

Electrical heater As already introduced in chapter 1, it consists in one or more discs located upstream the DOC that are heated up by current flowing in high-resistance circuits. The exhaust gas flow is rapidly heated up before proceeding along the exhaust line. It offers the great advantage of a fast heating that is independent

from engine operation and extremely focused on the target devices, enabling the actuation of an effective EATS thermal management with reduced wasted energy. A gas flow through the heating disc is mandatory to transfer the heating power to the following devices along the exhaust line, meaning that if a pre-heating phase is planned when the engine is still not running, a secondary air flow must be provided by installing an additional air pump.

DOC It promotes oxidation of exhaust components such as carbon monoxide (CO), unburned hydrocarbons (HC), and NO_x, using platinum-group metal (PGM)-based catalysts. The most common PGMs used in the DOC washcoat formulation are platinum, palladium and, less frequently, rhodium [3]. The DOC is typically the first component in a Diesel EATS and serves multiple functions, some of which are essential for the proper operation of the following aftertreatment devices. First, it converts any unburned species such as CO and HC to CO_2 and water. Second, since the reactions are exothermic, the heat generated can be used for raising exhaust temperature to trigger soot regeneration in the downstream particulate filter, or to enable earlier urea dosing for the SCR. Finally, the DOC oxidises NO to NO_2, to support both passive regeneration of the filter and to increase the rate of the SCR reaction through the "Fast SCR" mechanism, explained in the following paragraph. The overall oxidation reactions are:

$$2NO + O_2 \rightarrow 2NO_2 \tag{2.1}$$

$$4HC + 5O_2 \rightarrow 4CO_2 + 2H_2O \tag{2.2}$$

$$2CO + O_2 \rightarrow 2CO_2 \tag{2.3}$$

A detailed review on DOC chemistry, kinetic modelling, and issues connected to deactivation and poisoning can be found in [20].

SCR catalyst The SCR is a catalytic process of reduction of oxidised compounds (NO_x) in an environment in which oxygen presence is typically still abundant such as the exhaust stream of a lean combustion process, like the one happening in Diesel engines. Urea is usually the source of ammonia, used as the reducing agent needed

by the SCR process. In contrast to pure ammonia, used in static applications, a Diesel exhaust fluid (DEF), commercially known by the name AdBlue, is employed in mobile applications, mainly for safety and space reasons. Adblue is an aqueous solution of 32.5% by weight of high purity urea in deionised water that is injected and vaporized into the exhaust gas flow upstream of the SCR catalyst. Ammonia is then made available in the gas phase via the following set of reactions, including water evaporation (2.4), urea thermolysis (2.5) and isocyanic acid hydrolysis (2.6)([3]):

$$(NH_2)_2CO_{(aq)} \rightarrow (NH_2)_2CO_{(s/l)} + 6.9H_2O_{(g)} \tag{2.4}$$

$$(NH_2)_2CO_{(s/l)} \rightarrow NH_{3(g)} + HNCO_{(g)} \tag{2.5}$$

$$HNCO_{(g)} + H_2O_{(g)} \rightarrow NH_{3(g)} + CO_{2(g)} \tag{2.6}$$

The first part of the SCR system , where water in the exhaust reacts with the urea releasing ammonia according to reactions above, is called hydrolysis catalyst. The second stage is the actual SCR catalyst, where SCR process takes place converting NO_x to N_2, according to the following set of global reactions:

$$4NH_3 + 4NO + O_2 \rightarrow 4N_2 + 6H_2O \tag{2.7}$$

$$2NH_3 + NO + NO_2 \rightarrow 2N_2 + 3H_2O \tag{2.8}$$

$$8NH_3 + 6NO_2 \rightarrow 7N_2 + 12H_2O \tag{2.9}$$

The highest reaction rates are achieved in reaction (2.8), referred to as "Fast SCR", when an equimolar amount of NO and NO_2 are present in the exhaust gas. For this reason the DOC plays a key role in the NO_x reduction process, ensuring the oxidation of NO to NO_2. The amount of NH_3 supplied via control of the injected urea is adjusted to provide a modest excess above the amount required for the NO_2 and NO to be reduced to N_2. Therefore, the final stage of the SCR system consists in an oxidation catalyst, that removes any excess NH_3 by oxidizing it to N_2, according to the following reaction:

$$4NH_3 + 3O_2 \rightarrow 2N_2 + 6H_2O \tag{2.10}$$

More details concerning SCR chemistry can be found in [21]. A wide variety of catalysts have been developed in the past several years and continue to improve. Leading examples include the use of vanadia–titania, zeolites exchanged with base metals such as copper and iron, and metal oxides. The overall NO_x conversion efficiency can be very high over a specific operating temperature window that depends on the type of catalyst used, as illustrated in Fig. 2.3 [22].

Figure 2.3: Operating temperature windows for different SCR catalysts: NO_x conversion efficiencies as a function of catalyst temperature.

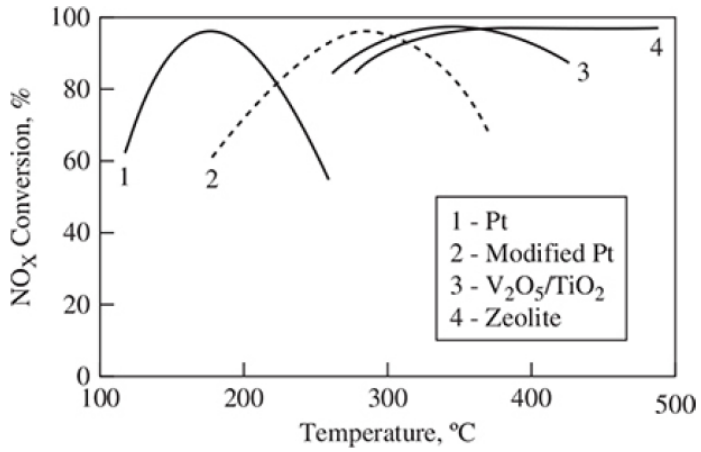

LTM-SCR catalyst It is an SCR catalyst with reduced thermal inertia and usually installed before the particulate filter in order to speed up the heating phase as much as possible and reach the light-off temperature in a shorter time. This allows to reduce NO_x emissions during engine cold start by limiting the time period in which SCR reactions can not take place due to low temperature.

SDPF SCR-coated Diesel particulate filters constitute an additional strategy for dealing with high NO_x emissions during low-temperature operations. These filters consist of a wallflow monolith coated with materials that both enhance soot oxidation and reduce NO_x. Since it is placed nearer to the engine, the SDPF achieves a faster warm-up with respect to the standard SCR unit placed downstream the DPF. Typical materials used for simultaneously controlling NO_x and soot are rare

earth metal oxides, spinel-type oxides, hydrotalcites, perovskites, mixed transient metal oxides, and platinum-group metals. The effects of SCR reaction and ammonia on soot oxidation and, on the other hand, the influence of soot loading on NO_x reduction have been investigated in numerous studies, reviewed in [3].

2.2 *Simulink* model

Nowadays, model-based development in the automotive industry is widely adopted since this approach allows to reduce the so-called time to market by simplifying the validation process, in order to be competitive in the fast changing automotive market. The availability of a reliable simulation tool is a key enabler for the design and the optimization of complex systems such as HEVs. The adoption of a comprehensive 0D quasi-static vehicle model developed in *Matlab/Simulink* environment, as the one chosen for this application, is common practice when the main focus is to simulate fuel consumption, pollutant emissions or vehicle performance over long duration driving cycles, being a good compromise between simulation accuracy and computational time.

2.2.1 Model description

The vehicle model that has been adopted for the application discussed in this work is the result of the merging of two different previously validated models available from FEV libraries: a P2 PHEV analytical model, that is the overall model base architecture, and a P0 HEV map-based model, which provides a detailed engine and EATS model that is essential for the purposes of this activity. All vehicle and engine input data come from the map-based model just mentioned. The base analytical model architecture has been modified, if needed, to match with these input data. Finally, EM and HV battery data come from a previous benchmarking activitiy, as described below in the model validation section. A schematic representation of model architecture and data sources is given by Fig. 2.4.

The model is structured in modular blocks that are organized in different levels, so that a block can contain further sub-blocks modelling specific components or performing more specific functions. Each block has its own input and output signals and

Figure 2.4: Schematic representation of model architecture including main physical and controller subsystems

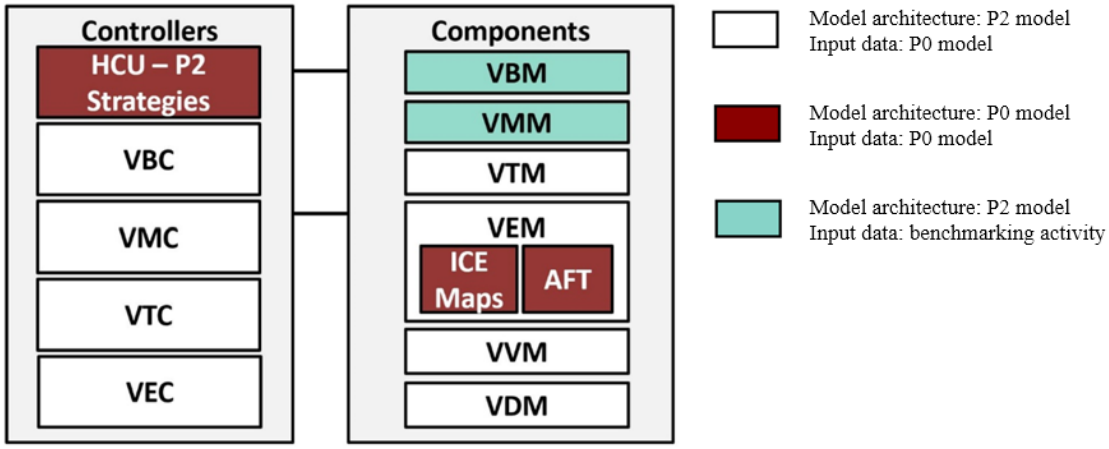

all blocks are connected between each other through a bus creator that transmits all the signals. The model top layer is organized in three different sub-systems: physical, controller and scope subsystem. The first two subsystems contain respectively all vehicle components physical models and corresponding control units, while the third one allows to visualize all the main signals that can be useful for monitoring the model.

Below is an overview of the main functions and equations modelled in each block inside physical and controller subsystems.

Vehicle physical subsystems

Vehicle model (VVM) It models vehicle dynamics taking into account only the longitudinal forces acting on the vehicle. Vehicle longitudinal dynamics is described by the following equations:

$$m_v \frac{d}{dt} v(t) = F_t(t) - F_{res}(t) \tag{2.11}$$

$$F_{res}(t) = F_a(t) + F_r(t) + F_g(t) \tag{2.12}$$

where m_v is the vehicle mass, v is the actual vehicle speed, F_t is the propulsion force and F_{res} is the resistance force acting on the vehicle, calculated as the sum of aerodynamic, rolling and road gradient related resistance. Aerodynamic and rolling resistance forces depend on vehicle speed and they are modelled through experimental coast-down coefficients f_0, f_1 and f_2, so that total resistance force becomes:

$$F_{res}(t) = f_0 + f_1 v(t) + f_2 v^2(t) + m_v g \cdot sin\alpha(t) \tag{2.13}$$

where α is the road slope. Another important output of this block, together with vehicle actual speed and acceleration, is maximum wheel torque request, which is calculated according to grip limitations.

Figure 2.5: Longitudinal forces acting on a vehicle in motion

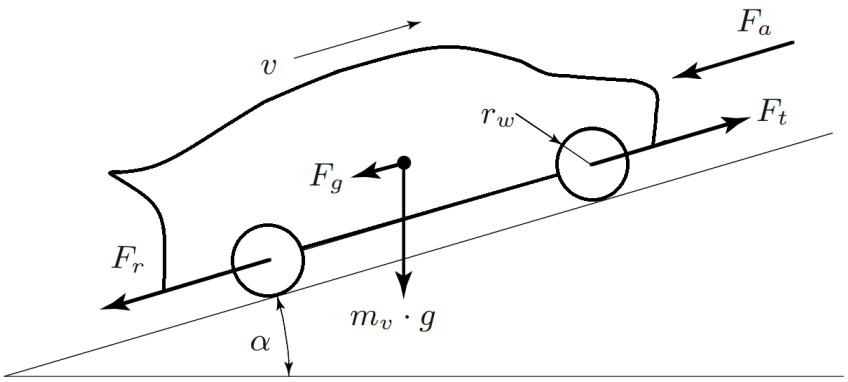

Driver model (VDM) It contains information about the drive cycle we want to perform, in terms of speed profile and road gradient over time, and simulates the driver behaviour. Requested torque at the wheels T_{req} in order to follow the speed profile is calculated through the equations:

$$F_{req}(t) = F_{res}(t) + (m_v + m_{eq,rot}) \cdot \frac{d}{dt} v_{req}(t) \tag{2.14}$$

$$T_{req}(t) = F_{req}(t) \cdot r_w \tag{2.15}$$

where F_{req} is the total force requested at the wheels, $m_{eq,rot}$ is the equivalent mass of rotative components, r_w is the dynamic wheel radius and v_{req} is the vehicle speed

imposed by the drive cycle. Then a PI controller simulates the driver action in terms of positive or negative torque request to perform an acceleration or a braking action, based on the difference between requested speed and actual vehicle speed feedback. More in detail, braking torque request $T_{brk,ct}$ after controller intervention is calculated using the following equation:

$$T_{brk,ct} = (v_{req} - v_{act}) \cdot f_{P,brk} + f_{I,brk} \cdot \int (v_{req} - v_{act}) \cdot dt \tag{2.16}$$

where $f_{P,brk}$ and $f_{I,brk}$ are the proportional and integral factor for the PI controller, while v_{req} and v_{act} are the vehicle speed requested by the drive cycle and the actual speed respectively. The integral in (2.16) is reset whenever actual vehicle speed drops below a specific threshold. On the propulsion side, the PI controller adjusts the torque requested at the wheels, calculated as in (2.15), based on the error between requested and actual vehicle speed:

$$T_{req,ct} = (v_{req} - v_{act}) \cdot f_{P,acc} + f_{I,acc} \cdot \int (v_{req} - v_{act}) \cdot dt \tag{2.17}$$

being $T_{req,ct}$ the torque requested at the wheels after the PI controller intervention and $f_{P,acc}$ and $f_{I,acc}$ the proportional and integral factors of the controller as seen in (2.16).

Engine model (VEM) It contains a map-based physical engine model providing engine actual torque and speed based on different operating conditions and engine torque request coming from the engine control unit (ECU), taking into account inertia effects; a thermal model simulates the heat-up of oil, coolant and engine block, while fuel flow, pollutant emissions and exhaust gas temperature maps allow to calculate fuel consumption, engine-out emissions HC, CO, soot and NO_x and turbine inlet temperature as function of engine temperature, load and speed. Finally, CO_2 emitted is calculated starting from fuel consumption as follows:

$$\dot{m}_{CO_2}(t) = \frac{\dot{m}_{fu}(t)}{\rho_{fu}} f_{CO_2} \tag{2.18}$$

where $\dot{m}_{CO_2}$ is the CO_2 mass flow, $\dot{m}_{fu}$ and ρ_{fu} are fuel mass flow and density respectively and f_{CO_2} is a factor expressed in [g/l] corresponding to the amount of CO_2 deriving from the combustion of one litre of fuel, directly related to the type of fuel considered and calculated according to the the European Regulation No 2017/1151 [23].

EATS model Each component is modelled as a separate block and connected to the others to form the complete exhaust line. Thermal heat exchange with the exhaust gas is modelled in each block by dividing the physical component into a series of elementary bricks in which the contributions of conduction, radiation, external and internal convection are calculated separately using semi-empirical formulas to determine the temperature of the solid material of the brick and of the exhaust gas at the brick outlet. The equations implemented in each brick describing the heat exchange are described below.

The heat exchanged by internal convection $\dot{Q}_{conv,int}$ is given by the following equation:

$$\dot{Q}_{conv,int} = h_{int} \cdot A_{int} \cdot \left(T_{gas,0} \frac{\epsilon_s}{1 + \frac{\epsilon_s}{\epsilon_t} - \epsilon_s} - T_{solid,0} \frac{\epsilon_t}{1 + \frac{\epsilon_t}{\epsilon_s} - \epsilon_t} \right) \tag{2.19}$$

where A_{int} is the internal brick surface in contact with the gas, $T_{gas,0}$ and $T_{solid,0}$ are the initial temperatures of the gas and of the solid material respectively, while the parameters ϵ_s and ϵ_t are calculated for each brick as described in [24]. Finally, h_{int} is the convective heat transfer coefficient (HTC), obtained as:

$$h_{int} = \frac{Nu \cdot \lambda_{gas}}{d} \tag{2.20}$$

being λ_{gas} the thermal conductivity of the considered gas, d the diameter of the cross section and Nu the Nusselt number, calculated as a function of Reynolds number Re according to Meisner-Sorenson relation:

$$Nu = 0.077 \cdot Re^{0.769} \tag{2.21}$$

The temperature of the gas at the brick outlet $T_{gas,out}$ is calculated as:

$$T_{gas,out} = T_{gas,0} - Nu_t \cdot \left(T_{gas,0} \frac{\epsilon_s}{1 + \frac{\epsilon_s}{\epsilon_t} - \epsilon_s} - T_{solid,0} \frac{\epsilon_t}{1 + \frac{\epsilon_t}{\epsilon_s} - \epsilon_t} \right) \tag{2.22}$$

where Nu_t is the corrected Nusselt number, calculated as suggested in [25] to improve model behaviour during transients.

The average temperature of the solid material $T_{avg,solid}$, that is used to evaluate the other types of heat exchange, is obtained through the following equation:

$$T_{avg,solid} = T_{avg,gas} + \epsilon_t \cdot (T_{solid,0} - T_{avg,gas}) \tag{2.23}$$

where $T_{avg,gas}$ is the average temperature of the gas crossing the brick, calculated as:

$$T_{avg,gas} = \frac{T_{gas,0} + T_{solid,0} \cdot (\frac{\epsilon_t}{\epsilon_s} - \epsilon_t)}{1 + \frac{\epsilon_t}{\epsilon_s} - \epsilon_t} \tag{2.24}$$

The heat exchanged by external convection $\dot{Q}_{conv,ext}$ between the solid material and the surrounding environment is evaluated as follows:

$$\dot{Q}_{conv,ext} = h_{ext} \cdot A_{ext} \cdot (T_{amb} - T_{avg,solid}) \tag{2.25}$$

where h_{ext} and A_{ext} represent the convective HTC and the heat transfer area respectively, while $T_{amb} - T$ is the ambient temperature.

The contribution of radiation $\dot{Q}_{rad}$ is calculated as:

$$\dot{Q}_{rad} = \sigma \cdot \epsilon \cdot A_{ext} \cdot (T_{amb}^4 - T_{avg,solid}^4) \tag{2.26}$$

where σ is the Stefan-Boltzmann constant and ϵ is the emissivity.

The heat transferred by conduction $\dot{Q}_{cond}$ through the bricks is obtained through the following equation:

$$\dot{Q}_{cond} = \frac{\lambda_{solid} \cdot A_{cond}}{l} \cdot (T_{avg,solid,i-1} - 2T_{avg,solid,i} + T_{avg,solid,i+1}) \tag{2.27}$$

where λ_{solid} is the thermal conductivity of the solid material of the brick, A_{cond} is the contact area between the bricks and l represents the length of the considered

brick.

Once calculated all the contributions, the total heat flow $\dot{Q}_{tot}$ is defined as:

$$\dot{Q}_{tot} = \dot{Q}_{conv,int} + \dot{Q}_{conv,ext} + \dot{Q}_{rad} + \dot{Q}_{cond} \tag{2.28}$$

which allows to calculate the final temperature $T_{solid,fin}$ of the solid material at the end of the simulation step:

$$T_{solid,fin} = T_{solid,0} + \frac{\dot{Q}_{tot}}{m \cdot c_p} \tag{2.29}$$

being m the mass of the considered solid material and c_p the corresponding specific heat capacity.

As already mentioned, the base architecture of the heat transfer model is the same for each component of the exhaust line, adjusting all the coefficients for each specific component and taking into consideration also the contribution of any exothermic chemical process that may happen due to the conversion of pollutant species.

DOC conversion efficiency maps of HC, CO and NO as function of volumetric flow rate and gas average temperature allow to calculate the resulting pollutant emissions after the oxidizing reactions happening in the DOC. NO_x reduction performed by LTM-SCR, SDPF and SCR is modelled for each device by firstly calculating NO_x conversion efficiency, which depends on gas average temperature, NO_2/NO_x ratio and space velocity, given by the ratio between the volumetric flow rate of the reactants and the volume of the reactor; then, from the knowledge of conversion efficiency, it is possible to obtain the amount of NH_3 that can actually react to reduce NO_x, and so the amount of Adblue to be injected.

The electrical heater is modelled as one single brick, following the same equations already discussed above to calculate the temperature of the exhaust gas flow at the outlet. In this case, an additional contribute to the power balance is given by the electric power employed to heat up the device and then transferred to the exhaust gas flow through internal convection.

Transmission model (VTM) A physical transmission model calculates the torque transmitted through the launch clutch, between the electric motor and the gearbox, and the separation clutch, between the engine and the electric motor, according to clutch states (locked, unlocked, slip control). A second subsystems represents transmission thermal model, in which also transmission efficiency is calculated using a map-based approach depending on temperature, torque and active gear. A state machine performs the gear change when requested.

EM model (VMM) The model accounts for the calculation of motor speed, torque and actual electric power consumption, based on torque request coming from the EM controller, considering inertia losses and eventually engine drag torque. The core is made by experimental efficiency maps, which are used to take into account the EM losses both in motor and generator mode as function of speed and load. Motor efficiency is then used to calculate the electric energy requested to the HV battery, based on the mechanical and electrical power balance, as follows:

$$\begin{cases} P_m = 2\pi \cdot T_{mot,act} \cdot \frac{n_{mot,act}}{60} \\ P_{el} = P_m \cdot \eta_c^k \cdot \eta_m^k \end{cases} \tag{2.30}$$

where P_m is the mechanical power, $T_{mot,act}$ is the actual motor torque and $n_{mot,act}$ is the actual motor speed. On the electric side, η_c is the inverter efficiency, η_m is the mechanical efficiency, k is a constant, equal to -1 when the EM operates as a motor and equal to 1 when it operates as a generator) and P_{el} is the electric power request sent to the HV battery. Finally, the electric motor rotational speed is computed starting from actual vehicle speed v_{act} through the following equation:

$$n_{mot,act} = \frac{v_{act}}{r_w} \cdot \tau_{gr} \cdot \tau_{fd} \tag{2.31}$$

being r_w the dynamic wheel radius, τ_{gr} the current gear ratio and τ_{fd} the final drive ratio.

High Voltage (HV) battery model (VBM) The physical component is modeled through an equivalent RC circuit that allows to calculate battery voltage V_{bat}

and current I_{bat} through the following equations system:

$$V_{bat}(t) = (V_{cel,OC}(T,SoC) - R_{cel,int}(T,SoC) \cdot I_{bat}(t)/n_p) \cdot n_s \tag{2.32}$$

$$P_{bat}(t) = V_{bat}(t) \cdot I_{bat}(t) \tag{2.33}$$

where n_p, n_s are the number of parallel and series cells, P_{bat} is the battery power request coming from the electric motor and the DC/DC converter, $R_{cel,int}$ and $V_{cel,OC}$ are respectively cell internal resistance and open circuit voltage, which are obtained from experimental maps as function of temperature and SoC. Power losses due to resistive heating are then calculated as follows:

$$P_{bat,loss}(t) = V_{bat,int} \cdot I_{bat}(t) \tag{2.34}$$

$$V_{bat,int} = \frac{n_s}{n_p} R_{cel,int}(T,SoC) \cdot I_{bat}(t) \tag{2.35}$$

where $V_{bat,int}$ is the internal voltage drop due to battery internal resistance. Battery actual state of charge SoC is determined through the following equation:

$$SoC(t) = SoC_0 - \frac{\int_0^t I_{bat}(t)\, dt}{C_{bat}} \tag{2.36}$$

where SoC_0 is the initial state of charge and C_{bat} is the nominal battery capacity. A thermal model calculates battery temperature depending on power losses and thermal exchange with air and coolant.

DC/DC converter model It translates the power requested to the 12 V battery into power requested to the HV battery to maintain a fixed SoC of the 12 V battery, taking into account its efficiency.

12V battery model The physical representation is quite similar to that of the HV battery.

Junction box model It represents the physical connection between all HV consumers, in this case the electric motor and the DC/DC converter.

Figure 2.6: Equivalent circuit for cell electrical characterization

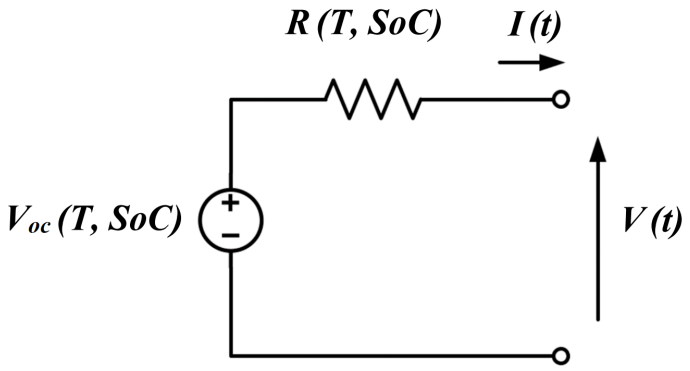

Vehicle controller subsystems

Hybrid control unit (HCU) It controls powertrain operation and acts as a supervisor for all the other slave controllers. First of all, a specific function determines the driving mode between pure electric drive (e-drive) or hybrid mode, according to the implemented hybrid strategy. Hybrid mode is further divided into different powertrain operating modes including engine start phase, engine load point shift, range extender mode and engine stop phase. Another function evaluates the negative torque requested to the electric motor according to the driver request, and eventually sends the additional brake torque request to the vehicle model, so that regenerative braking is always maximized according to electric motor and battery limits. Engine and motor torque request are determined according to the operating mode and sent to the corresponding controllers. Another block calculates the requested gear according to the adopted shifting strategy based on speed thresholds maps depending on vehicle speed and requested torque.

Engine controller model (VEC) The first of the different functions included in the ECU model gives information about the current engine status depending on operating conditions (e.g. start, stop, idling, fuel cut-off etc.); another function acts on engine torque request according to HCU request taking into account engine operating mode, idle speed control and torque limitations; the final torque request

includes also engine friction losses and cold start measures (e.g. cat-heating) that are modelled as two further subfunctions.

Transmission controller (VTC) It controls through a state machine the operating conditions of both launch and separation clutch, according to requested torque, engine and motor states and speed, shifting request and transmission torque limits.

Electric motor controller (VMC) It contains limitations on the torque requested to the electric motor, obtained from motor continuous and peak torque curves. A state machine determines motor operating modes preventing it to work in peak operation for too long, which in reality can cause overheating issues and consequent power limitation;

Battery controller (VBC) It contains map-based power limitations according to battery peak or continuous operation modes.

2.2.2 Model validation

In order to have a robust and reliable simulation tool, providing results in terms of fuel consumption and pollutant emissions which are comparable to real values, the most significant quantities involved in a hybrid electric powertrain, such as EM and ICE torque, battery current and SoC must be simulated and compared with experimental results. Since the described model is not representing an actual existing vehicle, a comprehensive vehicle model validation would not be possible due to the lack of experimental data. Therefore, already existing validations of the adopted models for vehicle dynamics, electric power unit, engine and aftertreatment system will be individually presented in the following paragraphs.

EM and HV battery models

As fully described in [26], vehicle dynamics, EM and HV battery models were validated for an existing P2 PHEV along a WLTC cycle performed in charge-depleting (CD) conditions, meaning that the vehicle performs the driving cycle starting with fully charged battery, which allows to complete the whole test in full-electric driving

mode with no engine intervention. To this regard, Fig. 2.7 shows that the driver is capable of following accurately the speed profile. Focusing on plot 2.8, it can be seen that the model is capable to accurately calculate EM torque and speed both in motoring and generator mode, showing very good agreement with the experimental data apart from a small overestimation of the regenerative contribution which can be noticed for negative torque values. Concerning the HV battery, even though a quasi-static model is not able to fully simulate fast transient phases, current and power (which have the same trend) are simulated with good accuracy, showing a good match with the measurements both for negative and positive current values. As a consequence, the simulated battery SoC trend matches very well the experimental one, both during charging and discharging phases.

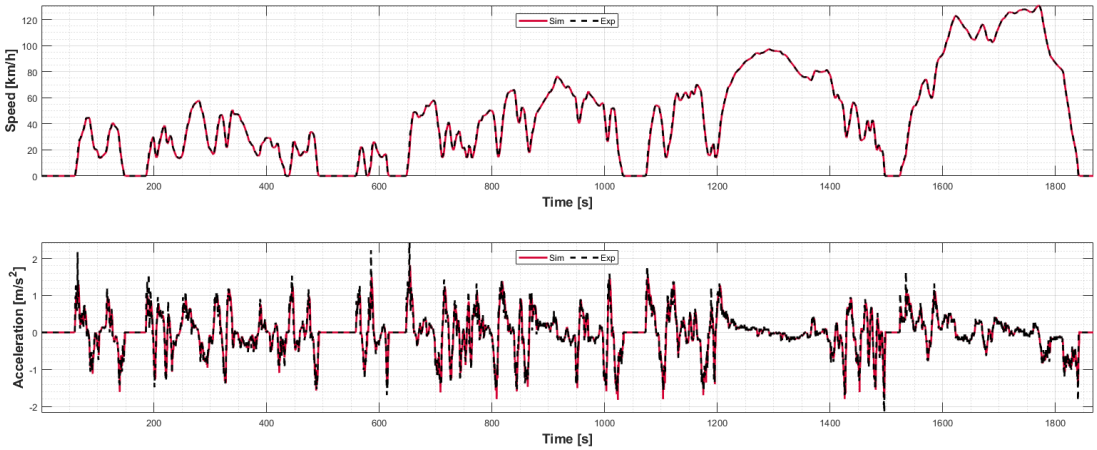

Figure 2.7: Vehicle model validation: experimental (black dashed) and simulated (red solid) results over a WLTC CD cycle.

ICE and EATS model

The map-based ICE and EATS models have been calibrated and validated as part of a previous project within FEV by comparing simulation and experimental results collected during tests on the chassis dynamometer.

As it can be noticed in Fig. 2.9 from the results of this validation process, both brake mean effective pressure (BMEP) and rotational speed are simulated quite accurately except for an underestimation in some peak values due to the quasi-static

nature of the model. According to the instantaneous and cumulated CO_2 profiles, the model is capable of reproducing pretty well the instantaneous CO_2 flow rate over the entire cycle; even if the experimental CO_2 peaks are not fully captured, the transient behaviour is balanced over the whole driving cycle so that the total CO_2 production is in good agreement with the experimental values. The same applies also for raw NO_x emission estimation.

Concerning the EATS model, experimental data, and thus direct validation, are only available for some specific tested layouts different from the one adopted in this activity. However, a modular modelling approach was adopted, so that the same modelled blocks representing each single component can be eventually combined to build several different EATS layouts depending on the specific application. This allows to derive the validation of each single component as part of a specific EATS layout that has actually been tested and directly validated. For this purpose, the comparison between simulated and experimental data related to two different EATS layout are provided in Fig. 2.10. Given the targets of this activity, the attention has been mainly focused on NO_x emission estimation and related quantities. The same considerations already made about engine-out emissions are also valid for tailpipe NO_x emissions, showing a good matching between simulated and experimental data in terms of cumulated emission, despite some inaccuracies concerning instantaneous quantities.

Focusing on the electrical heater, since experimental data were not available, a different type of validation has been proposed according to a previous activity carried out within FEV: output data coming from an electrical-heater validated model already available from GT-power libraries have been used as reference and compared with the ones provided by the considered *Simulink* model. The same input data in terms of air mass flow, electrical power and inlet temperature are supplied to both simulation platforms and exhaust gas temperature values at e-heater outlet are then compared (Fig. 2.11). Although some inaccuracies can be noticed especially during fast transients, the two sets of data follow the same general trend, which is considered acceptable within this implementation.

To summarize, with the adopted simulation approach, a realistic estimation of produced CO_2, engine-out emissions, EATS behaviour and thus NO_x tailpipe emission

is given. This level of accuracy is acceptable for the purpose of this activity, which is to highlight the potential of a predictive control strategy paired with a possible state-of-the-art PHEV in terms of NO_x emission reduction, rather than providing high precision results that will be otherwise mandatory if a real world application is expected.

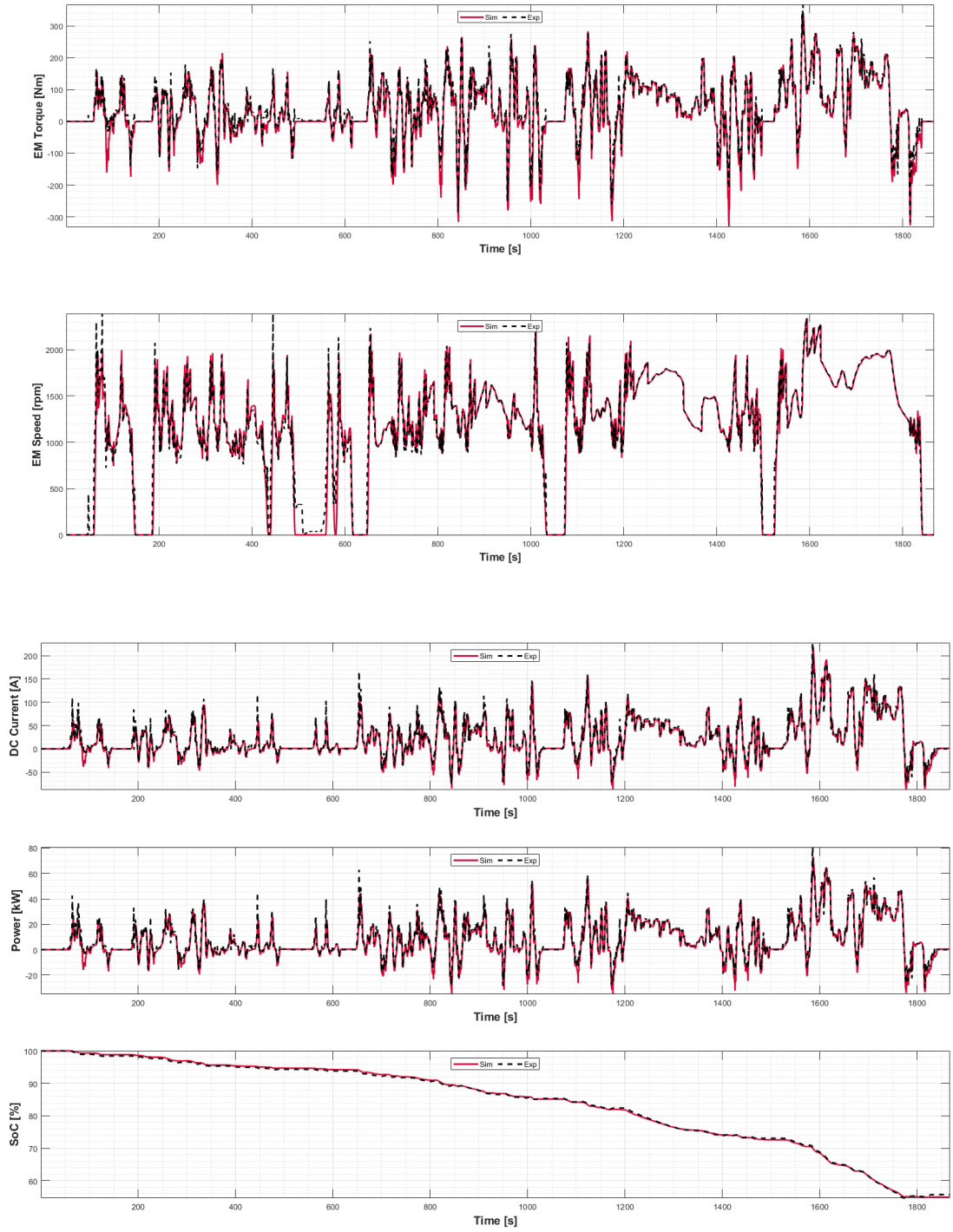

Figure 2.8: EM and HV battery model validation: experimental (black dashed) and simulated (red solid) results over a WLTC CD cycle.

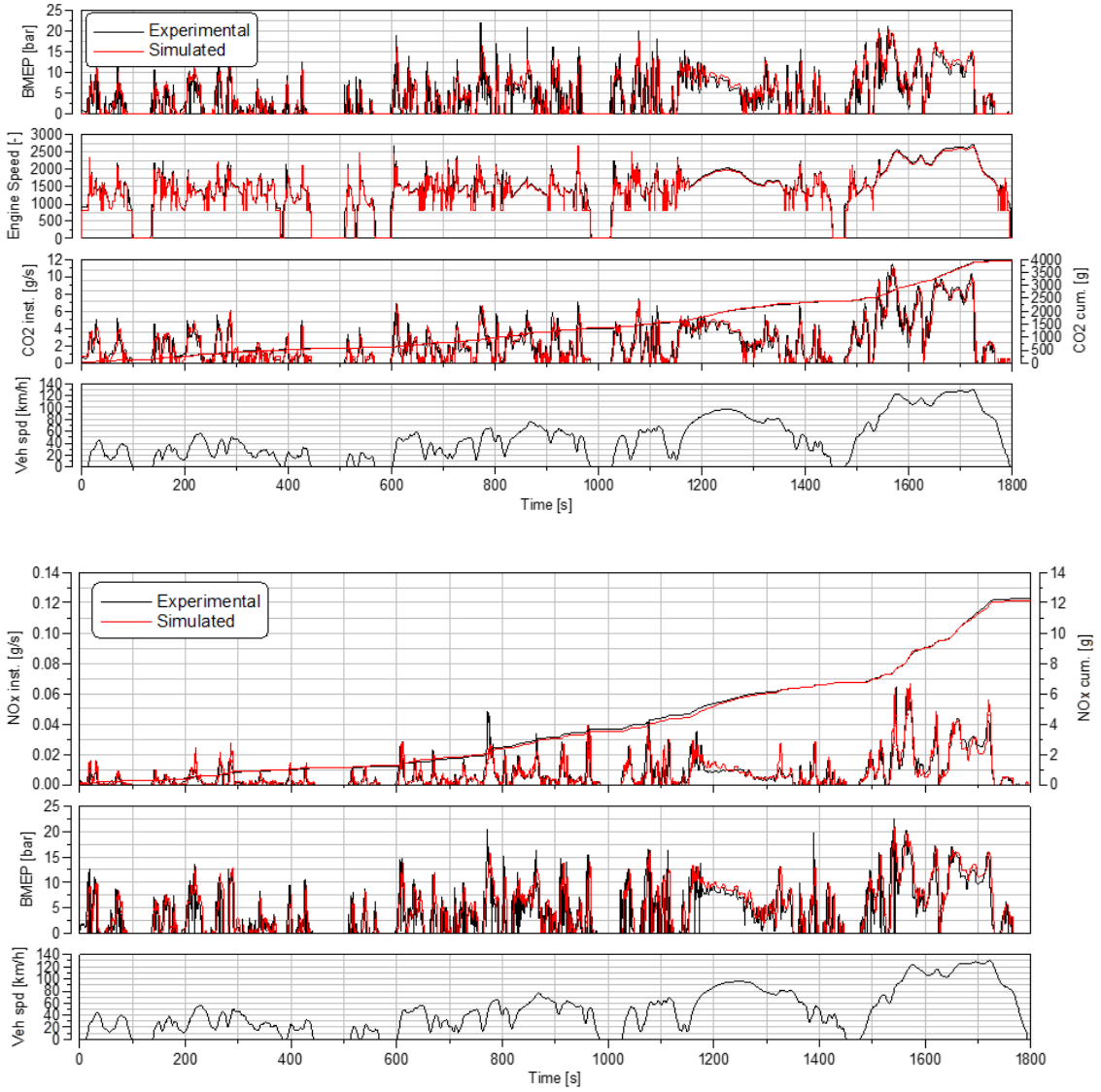

Figure 2.9: ICE model validation: experimental (black) and simulated (red) results over a WLTC cycle.

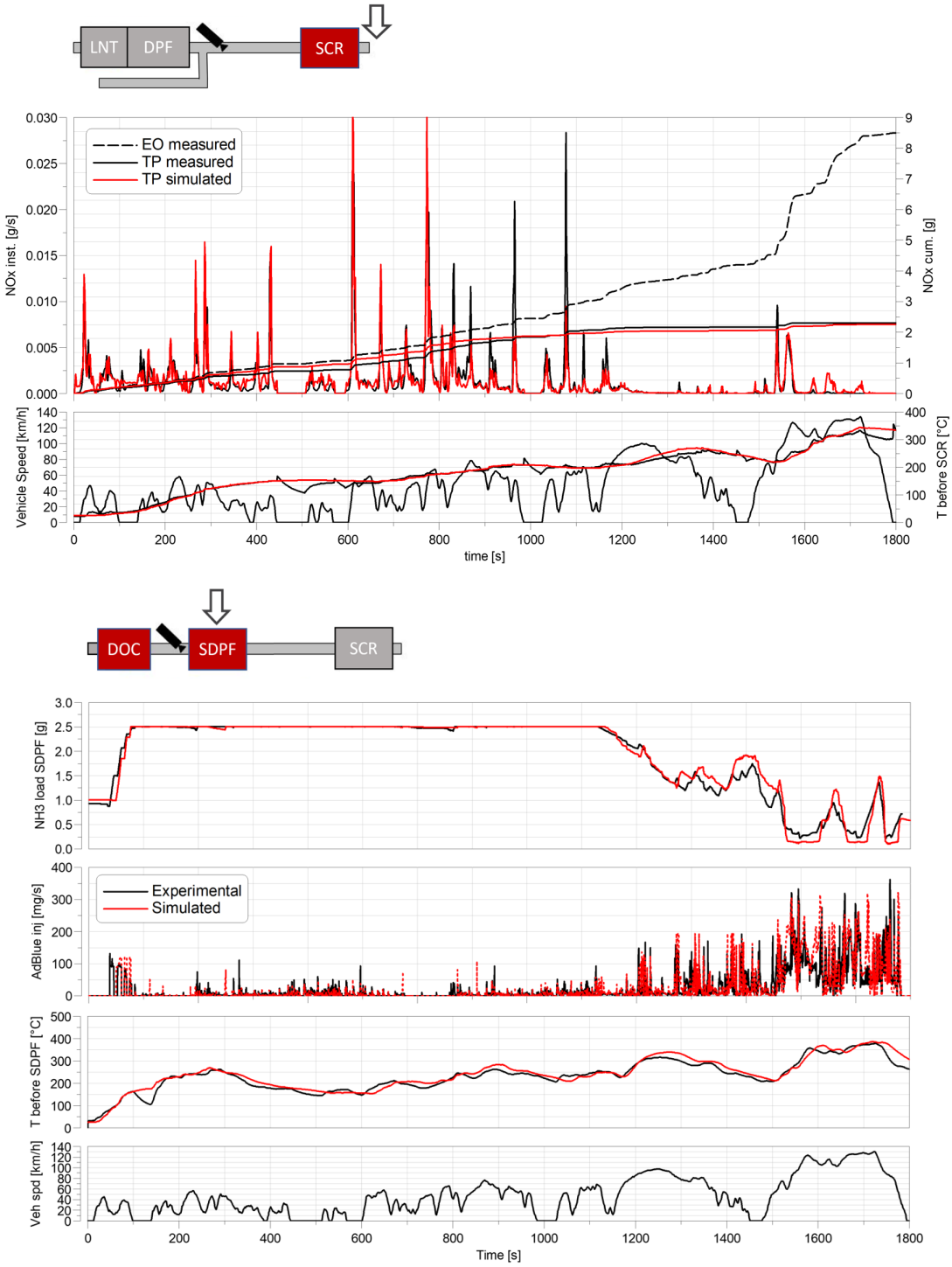

Figure 2.10: EATS components model validation: experimental (black) and simulated (red) results over a WLTC cycle. A schematic representation of the specific tested layout and measurement location is also provided.

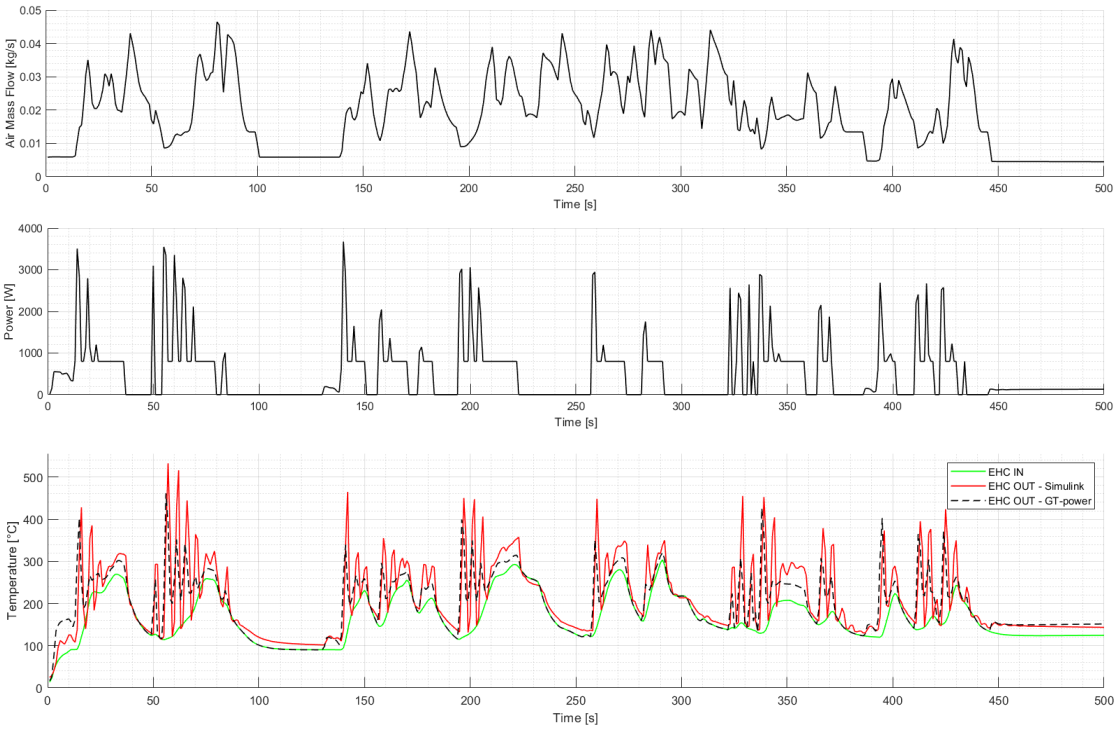

Figure 2.11: E-heater model validation: exhaust gas temperature at e-heater outlet from GT-power (black dashed) and Simulink (red solid) given the same input data.

Chapter 3

Control strategy development

In this chapter, as a first step the rule-based control strategies for the management of both hybrid powertrain and exhaust aftertreatment system are explained. In particular, the control strategy managing the driving mode and the torque split between EM and ICE is firstly investigated, followed by the description of the adopted rule-based strategy for the EHC thermal management. Then, a predictive control function based on the knowledge of the future driving path has been developed focusing on the EHC activation to perform a pre-heating phase before the first engine start, preventing low efficiency operation of the EATS.

3.1 Rule-based strategy

3.1.1 Torque split strategy

The development and calibration of a robust and effective control strategy is a preliminary step for the development of additional control functions involving EATS thermal management, taking advantage of the flexible hybrid architecture to reach the desired targets in terms of CO_2 and NO_x emissions.

The HCU is responsible for the selection of the driving mode between full electric drive (e-drive) and hybrid drive. Thus it manages the torque split between the EM and the ICE, taking into account several parameters that will be introduced in the next paragraphs.

Driving mode selection

The selection of the driving mode relies on a set of logical conditions enabling the switch from e-drive to hybrid drive and vice-versa:

- **Vehicle speed** E-drive is possible until actual vehicle speed is below a constant threshold which has been set to 140 km/h in compliance with EM technical specifications, allowing to perform a complete WLTC cycle in pure electric mode [23]. Over this speed threshold ICE intervention is required. A minimum hysteresis interval of 10 km/h has been introduced to avoid unstable behaviours of the model;

- **HV battery SoC** A constant threshold and related hysteresis have been set through a DoE approach in order to achieve the highest reduction of CO_2 emissions. The lower limit, below which ICE is switched on, and the upper limit, above which ICE is turned off, have been varied in the interval 18-26% considering all the possible combinations, that were tested over a complete WLTP standard procedure to evaluate equivalent CO_2 emissions. According to the results of the described analysis, graphically represented in Fig. 3.1, the selected lower and upper thresholds are 18 and 20% respectively;

- **ICE operating time** Minimum engine on and e-drive time intervals have been set to 10 seconds and 2 seconds respectively, in order to prevent too frequent ICE and EM starts and stops that would affect vehicle drivability;

- **EM torque request** A variable torque threshold, above which e-drive is no more possible, is calculated based on available EM continuous torque, which is a function of actual motor speed. This allows to use as much as possible the electric motor keeping a minimum torque reserve for engine start phases, corresponding to the additional available torque during motor peak operation;

- **DOC temperature** The switch from hybrid drive to e-drive is not possible until the DOC has reached its light-off temperature, corresponding to 180°C, above which conversion efficiency reaches its maximum value. This condition has been set to promote EATS heating up after engine cold start.

Figure 3.1: DoE analysis for SoC thresholds definition: resulting weighted CO_2 emission, selected configuration (green dot) and unviable configurations (red star).

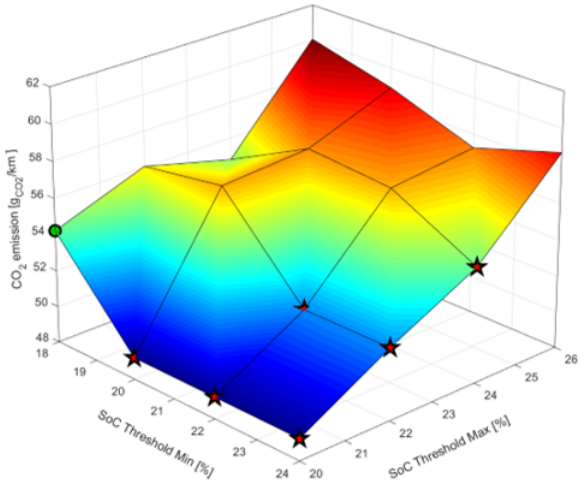

Load point shift maps definition

Focusing on hybrid mode, the torque split between ICE and EM is managed using a map-based approach. Load point shift (LPS) maps have been generated with three different targets depending on ICE operating conditions:

- Moving engine operating points to higher efficiency areas;
- Ensuring a minimum exhaust gas temperature in order to speed up the warm-up phases and keep a high EATS conversion efficiency during standard operation;
- Limiting NO_x emission during EATS warm-up when conversion efficiency is low.

Of course, different calibrations of the LPS strategy can be adopted depending on the set targets in terms of engine efficiency and pollutant emissions. Therefore, a preliminary step before the definition of the load point shift maps, was to define BSFC (Brake Specific Fuel Consumption), $BSNO_x$ (Brake Specific NO_x emission) and engine-out exhaust gas temperature optimal lines to be used as targets for the development of the load point shift strategy. These reference lines have been calculated based on engine fuel consumption, engine-out NO_x emissions and turbine

inlet temperature maps, as a function of engine speed and load. Considering the opposite trends of BSFC and $BSNO_x$ with engine load variation, BSFC and $BSNO_x$ targets must be set following a reasonable trade-off between the two trends, without focusing on a global minimization of one of the two that at the same time would strongly penalize the other. Engine-out exhaust gas temperature target must be set to a value that allows to heat up and keep the EATS within a temperature range that ensures high conversion efficiency, without affecting too much the BSFC.

Therefore, a DoE approach was used to calibrate the hybrid strategy by testing several configurations providing different results in terms of NO_x and CO_2 emissions. The WLTP standard test procedure [23] has been simulated to set $BSNO_x$ and exhaust temperature targets, evaluating average NO_x emission on the charge-sustaining reference cycle. This last procedure could not be used to set the BSFC target as well, since the corresponding LPS map is actually used only for the higher values of battery SoC, thus being irrelevant on a charge-sustaining cycle, as will be clarified in the next paragraphs. For this reason, an RDE cycle performed in charge-depleting mode has been considered to set the BSFC target separately from the other parameters, according to the best result achieved in terms of cumulative NO_x emission along the whole cycle. DoE parameters and resulting best configuration are listed in Tab. 3.1. In addition, Fig. 3.2 gives a graphical representation of the results obtained in terms of average NO_x and weighted CO_2 emission according to the WLTP procedure. As expected, the lowest average NO_x emission is obtained with a low $BSNO_x$ target and a high exhaust temperature target, but still ensuring limited CO_2 emission at the same time.

Table 3.1: Definition of DoE parameters range of variation.

Parameter	**Query points**	**Definition**	**Best**
BSFC target (k_{FC})	[1 1.03 1.05 1.08 1.1]	Relative increase with respect to minimum BSFC [-]	1.05
$BSNO_x$ target (k_{NOx})	[0 0.2 0.5 1 1.2 1.5 1.8 2]	Specific engine out NO_x emission [g/kWh]	0.2
T_{exh} target (k_T)	[230 250 270 300 320 350 370 400]	Engine-out exhaust gas temperature [°C]	370

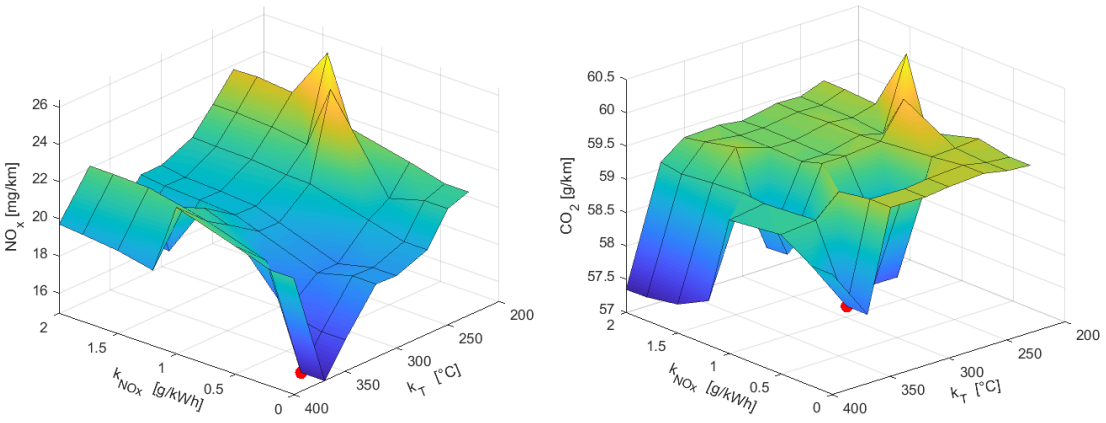

Figure 3.2: Results of DoE analysis for the definition of $BSNO_x$ and engine-out gas temperature targets: average NO_x emission (left), weighted CO_2 emission (right) and final selected configuration (red dot).

The resulting reference lines, obtained by following the mentioned targets for each engine operating condition, are shown in Fig. 3.3 and are the base for the definition of three different load point shift maps implemented in the model (3.4):

- **Normal mode shift-down** In this situation the electric motor provides part of the driving torque request, so that the engine works at lower load. The amount of torque requested to the electric motor is calculated in order to reach the BSFC target for each given engine speed. The aim is to reduce fuel consumption by using the electric motor;

- **Cat-heating mode shift-down** Similar to the previous one, but in this case the amount of torque requested to the electric motor is calculated in order to reach the $BSNO_x$ target for each engine speed. The aim is to reduce NO_x engine-out emissions while the EATS is cold and conversion efficiency is low;

- **Normal/Cat-heating mode shift-up** Additional torque is requested to the engine with respect to driving torque request and it is used to charge the battery. The additional torque value is calculated in order to follow the exhaust gas temperature target. The aim is to have a fast EATS heating and to keep it warm after the heating phase. In this case the load shift map is the same for both normal and cat-heating mode.

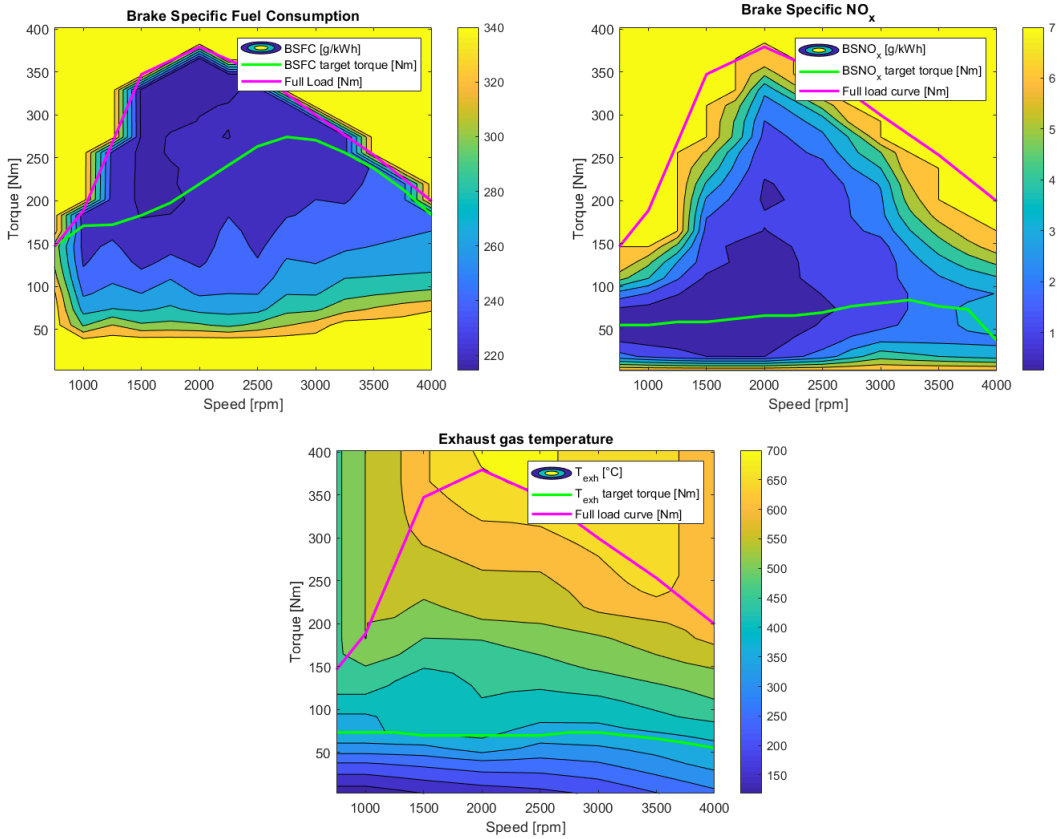

Figure 3.3: BSFC, $BSNO_x$ and exhaust gas temperature maps with corresponding defined targets.

The torque value coming from the LPS maps is then corrected through a multiplying factor that takes into account the battery SoC. The correction coefficients are defined together with each LPS map in order to decrease EM torque request if battery SoC is low or, on the other hand, to reduce the additional toque request to the engine if the battery is already charged (3.4). As it can be noticed, the correction factors for cat-heating mode are defined in order to make the engine operate at higher loads with respect to normal mode, leading to a faster warm-up phase.

3.1.2 EHC control strategy

The EHC control strategy is based on the following conditions, according to which the e-heater is activated if:

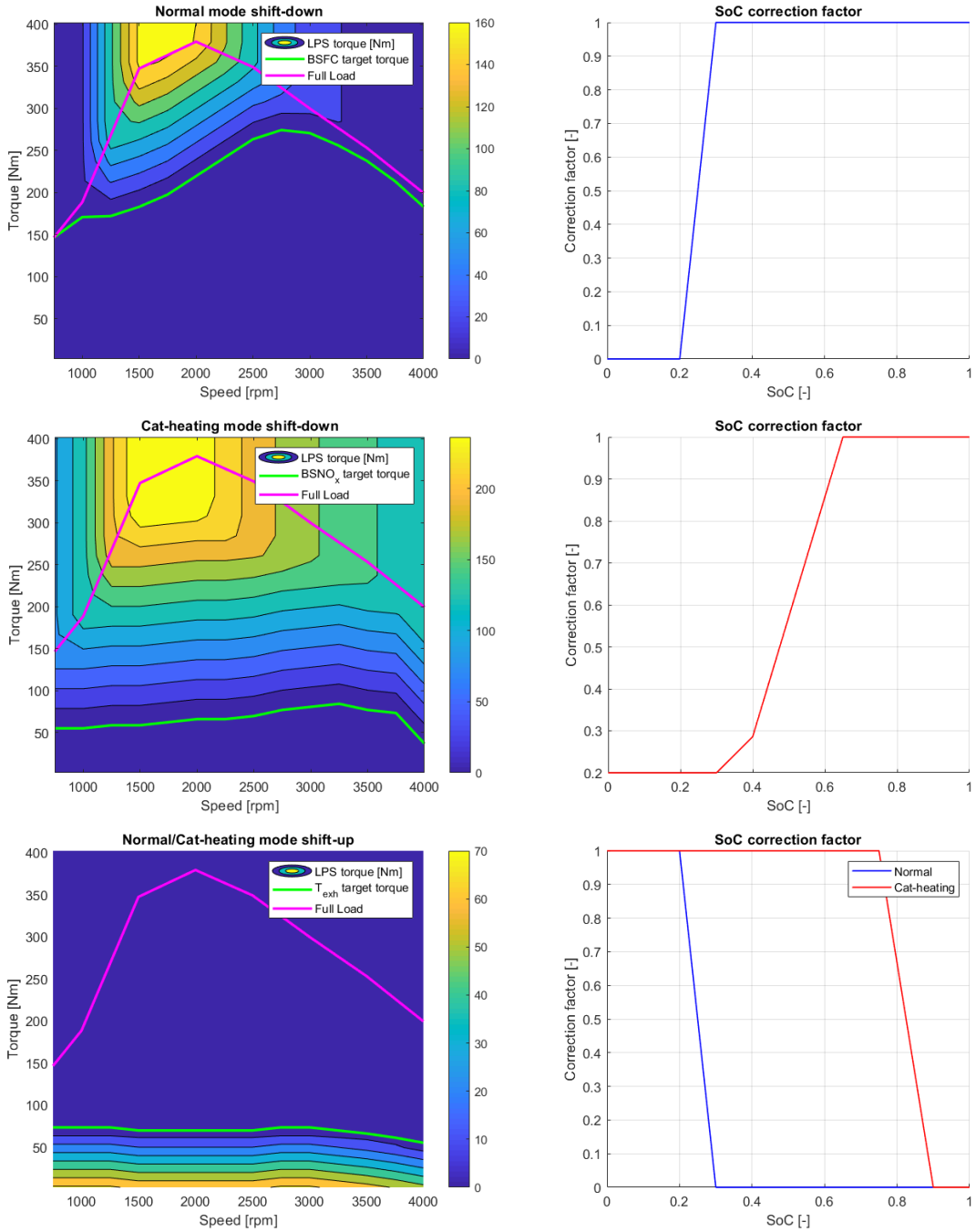

Figure 3.4: Load point shift maps for normal and cat-heating mode with the related SoC-based correction factors.

- the engine is running, meaning that the exhaust gas flow through the heating disc is not zero;
- the HV battery SoC is higher than a minimum safety threshold, that has been set to 15%;
- the exhaust gas temperature at DOC outlet is lower than a fixed threshold equal to 200°C, which is slightly above DOC light-off temperature.

Once the e-heater is activated, the requested power is calculated based on previously calibrated maps that take into account:

- actual engine load, which is directly connected to exhaust gas temperature;
- actual engine speed, that together with engine load allows to define the actual exhaust gas flow rate;
- actual exhaust gas temperature at e-heater outlet.

More in detail, electrical power is actually provided to the e-heater if engine BMEP is lower than 12 bar and if engine speed is lower than 2500 rpm, namely if engine-out exhaust gas temperature is below a certain threshold. Electrical power request is then calculated according to gas flow temperature at e-heater outlet, following the trend shown in Fig 3.5.

Figure 3.5: EHC power request as function of exhaust gas temperature at e-heater outlet.

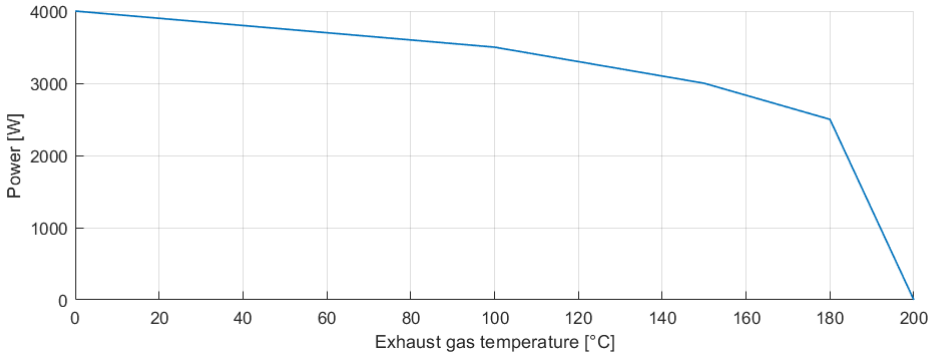

The advantages that can be achieved in terms of NO_x emission reduction by adopting an EHC managed with a simple rule-based strategy are clearly presented in chapter 4.

3.2 Predictive strategy

As already introduced in chapter 1, the availability of real-time navigation data, sent to the vehicle by a map-service provider, allows the reconstruction of the future driving scenario (eHorizon), thus enabling the development of predictive control strategies aimed to the best results in terms of energy management and pollutant emission. In particular, the knowledge of future driving conditions can be used to predict ICE first start along the travelled route, which is a key enabler for the predictive thermal management of the EATS, allowing to perform a pre-heating phase that can be actually planned to avoid NO_x cold start emissions, which give a significant contribute to the total emission along the considered driving cycle.

3.2.1 Characterization of the EHC thermal model

A preliminary step for the development of an effective EHC control strategy was to determine the heating energy needed to heat up the EATS achieving the desired conversion efficiency. In this regard, several simulations have been performed varying the parameters introduced below, in order to evaluate their effect on the heating phase.

- **Secondary air flow rate** As already mentioned in chapter 2, a secondary air flow must be forced through the exhaust line to perform a pre-heating phase while the engine is not already running. In the considered layout this is achieved by means of a secondary air pump, that in real-world application would be installed upstream of the EHC; to analyse the effect on the heating phase, the air flow rate has been varied according to the technical data of 12 V secondary air pumps available on the market. The evolution of absorbed current and air flow rate as a function of pump pressure for different supply voltages is shown in Fig. 3.6;

- **E-heater power** It refers to the electric power actually provided to the heating disc of the EHC, limited to 4 kW, in accordance to the state of the art of 48 V EHC ([13]);
- **Pre-heating duration** Heating power and secondary air flow rate are kept constant for a certain time interval needed to overcome the thermal inertia of the EATS devices; pre-heating duration to reach the light-off temperature can vary from few seconds to few minutes depending on the target device, the adopted power and the provided secondary air flow.

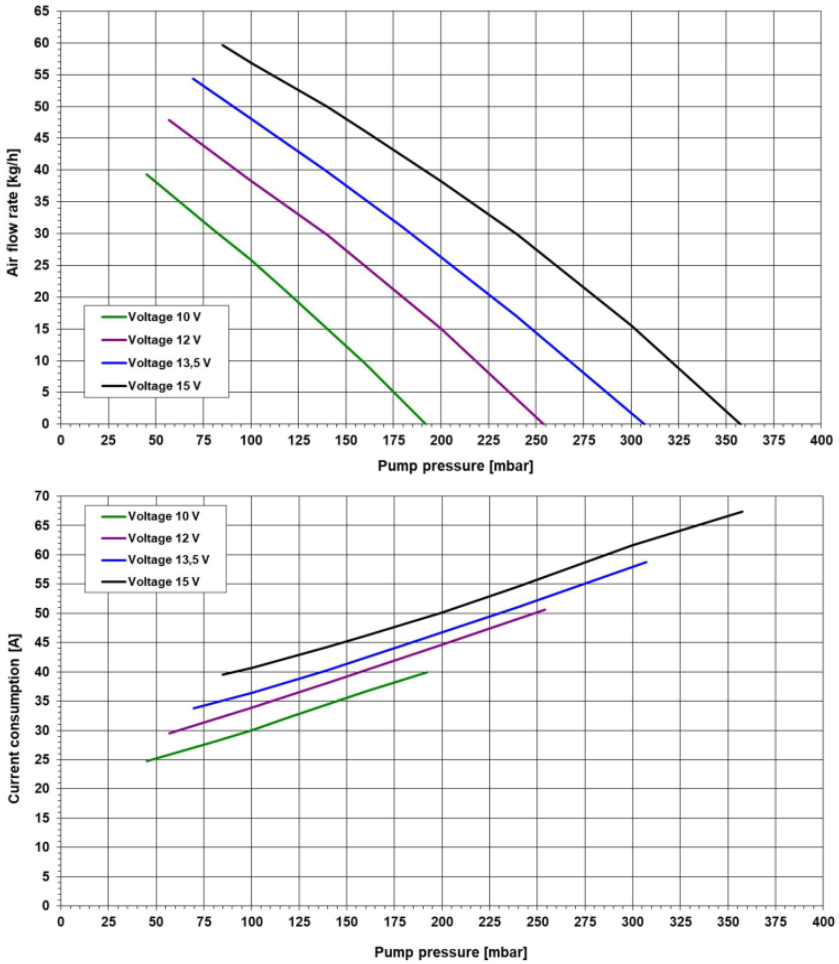

Figure 3.6: Secondary air pumps: air flow rate (top) and absorbed current (bottom) as a function of pump pressure for different supply voltages.

Sensitivity analyses of the main influencing parameters

A preliminary analysis has been carried out to evaluate the effects related to different values of provided power and air flow rate on DOC, LTM-SCR and SCR light-off time. More in detail, a fixed heating power and secondary air flow rate have been provided with the engine off in order to evaluate the only effect of EHC on the EATS heating phase. Then, the time needed to reach the light-off temperature, which has been set to 180°C for the DOC and 220°C for the SCR catalysts according to the respective pollutant conversion efficiencies, has been evaluated for the mentioned devices. The results, graphically represented in Fig. 3.7, clearly point out that the light-off time of all the devices decreases with increasing power and air flow rate, so that the same result can be achieved with different combinations of the considered parameters. It can be also noticed that the effect of an increasing air flow rate on the light-off time is more evident for the lower values of provided power and, in addition, the light-off temperature can not be reached at all under a certain minimum threshold of secondary air flow rate and heating power, especially referring to the SCR catalyst.

Further simulations have been run under the same conditions just mentioned for the previous analysis, aimed at evaluating the effect of the considered parameters on the maximum temperature reached by each device along the exhaust line. For this purpose, the evolution in time of the exhaust gas temperature at DOC, LTM-SCR and SCR outlet for two different heating power values (2 kW and 4 kW) has been reported in Fig. 3.8 for variable air flow rates. What can be deduced from the simulation results is that the maximum temperature reached by each device is directly related to the heating power, while the air flow rate has not significant influence from this point of view for both DOC and LTM-SCR, being more related to the heating time needed to reach a certain temperature rather than to the maximum temperature reached itself. This is not true in the case of the SCR catalyst, for which the air flow rate gains importance not only in terms of heating time but also of maximum temperature that can be reached. Besides this, another important conclusion is that, generally speaking, the influence of the air flow rate on the heating time grows from the start to the end of the exhaust line, making it necessary to

provide a significant secondary air flow in order to limit the heating time needed, especially if the target devices are the two SCR catalysts.

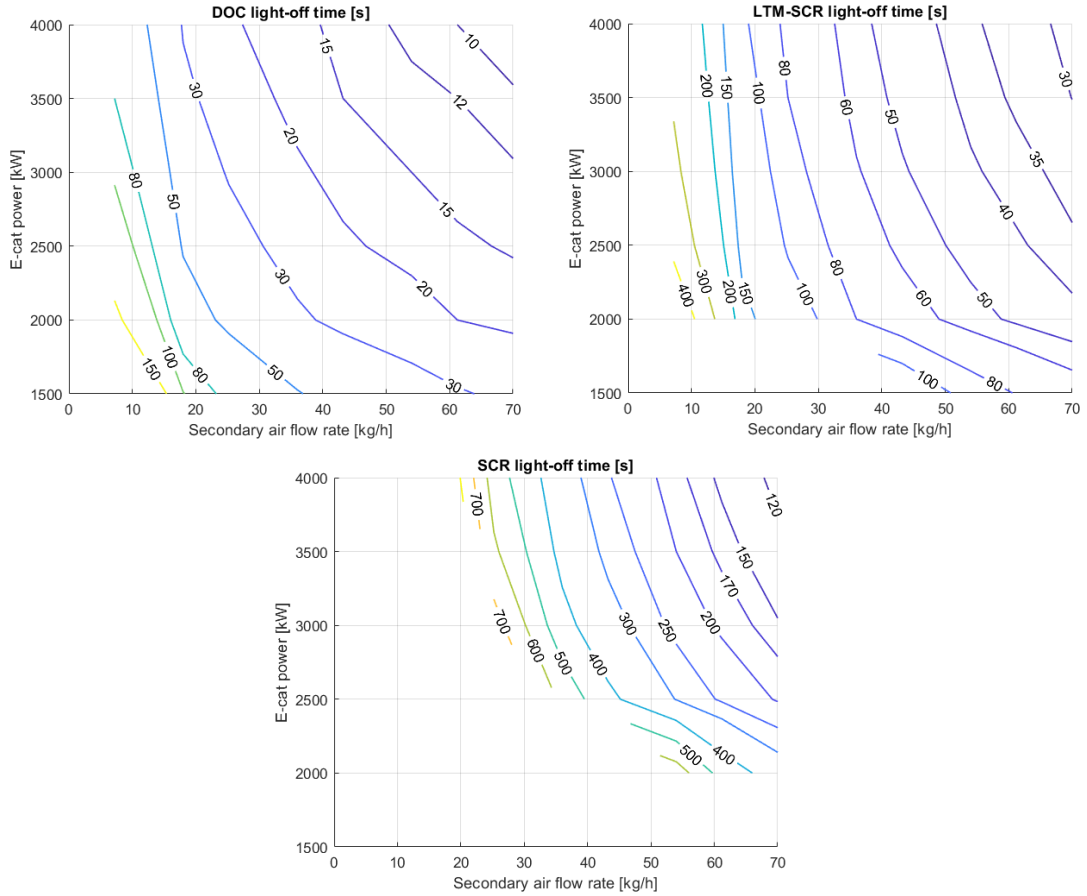

Figure 3.7: DOC, LTM-SCR and SCR light-off time as a function of secondary air flow rate and EHC power.

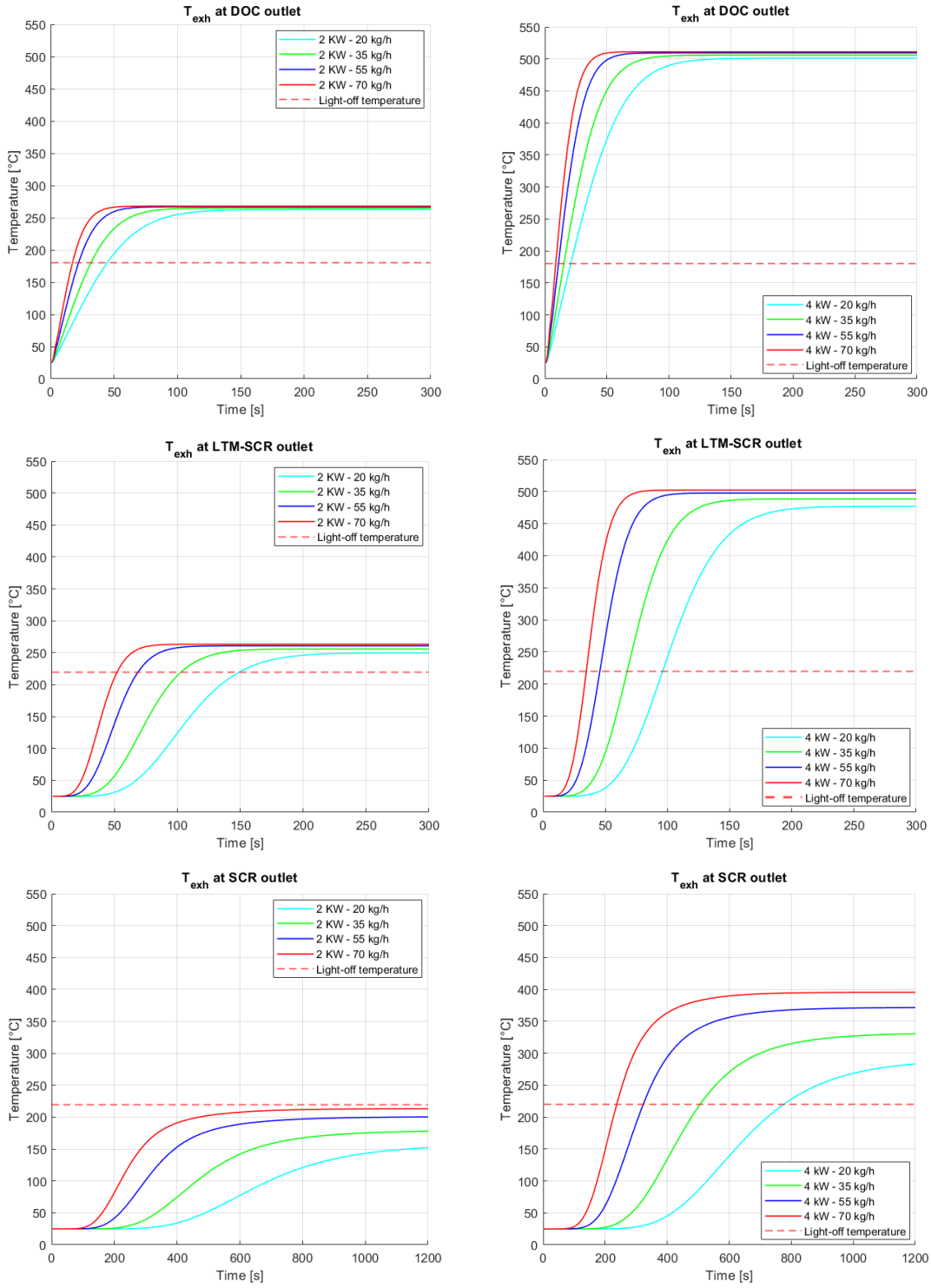

Figure 3.8: DOC, LTM-SCR and SCR temperature profiles for 2 kW (left) and 4 kW (right) e-heater power for variable air flow rates.

Pre-heating strategy definition

The preliminary analyses described above have been useful to set a lower threshold for each of the mentioned parameters to be taken into consideration for the following tests. Based on this, different configurations in terms of heating power and secondary air flow have been tested on an RDE cycle with increasing pre-heating time. The focus is the urban part of the driving cycle, as it will be defined in chapter 4, which is actually the most demanding from the point of view of pollutant emissions, due to engine cold start and low load operation, which means low EATS temperature and thus low NO_x conversion efficiency. The initial SoC has been set to 22% arbitrarily, in order to force ICE start due to low SoC along the considered driving cycle.

The pre-heating phase has been planned based on the a priori knowledge of the exact time instant in which ICE start happens, obtained by previous simulations. In particular, increasing values of heating power and secondary air flow rate have been tested, starting from minimum thresholds of 2 kW and 20 kg/s respectively, below which it is not possible to achieve the light-off of the DOC and especially of the LTM-SCR in a reasonable time, as evidenced in Fig. 3.7. The maximum air flow rate considered is 55 kg/h, accordingly to secondary air pump technical specifications, as previously mentioned. The minimum pre-heating duration taken into consideration is 30 seconds, based on the previous analysis as well. Concerning the upper limit for the heating power, a lower value with respect to the maximum allowed by state-of-the-art diesel EHC (4 kW) has been considered; the reason that led to this conclusion is related to the excessive temperature peaks that would be reached by the DOC and the LTM-SCR during the pre-heating phase. In fact, although a higher power leads to a faster warm up phase for a fixed air flow rate, it also leads to higher temperature peaks reached by these devices during the time interval needed to achieve a suitable operating temperature of the SCR catalyst. As seen in Fig. 3.8, the temperature at the DOC can reach more than 500°C if the maximum heating power is provided, and this would lead to issues like DOC poisoning, thermal ageing and decreasing NO to NO_2 conversion efficiency, which is fundamental to promote SCR reactions, as already explained in chapter 2. For this reasons, the maximum heating power has been limited to 3 kW.

Starting from these considerations, a DoE approach has been adopted to find

the most convenient pre-heating strategy in terms of resulting NO_x emissions and increased energy consumption due to the e-heater and the secondary air pump, the latter being calculated from the current consumption map shown in Fig. 3.6 depending on the supply voltage and the provided air flow rate. The boundaries set to define the range of variation of the DoE parameters are summarized in Tab. 3.2.

Table 3.2: Definition of DoE parameters range of variation.

Parameter	Limits	Motivation
EHC power	Lower limit: 2 kW Upper limit: 3 kW	SCR catalysts light-off DOC poisoning and NO oxidation
Secondary air flow	Lower limit: 20 kg/h Upper limit: 55 kg/h	SCR catalysts light-off 12V secondary air pumps specifications
Heating time	Lower limit: 30 s Upper limit: -	SCR catalysts light-off -

As expected, the best results in terms of absolute NO_x cumulative emission are achieved with the highest heating power and air flow rate. More in detail, Fig. 3.9 shows the results achieved by providing two different air flow rates, namely 45 and 55 kg/h, with variable heating power and time. What can be noticed is that almost the same reduction of NO_x cumulative emission, compared to the base configuration with no pre-heating, can be achieved with the highest heating power (3 kW) and a lower air flow rate (45 kg/h) or, on the contrary, with a lower heating power (2.5 kW) but an increased air flow rate (55 kg/h). The last option is more convenient from an energy consumption point of view: in this case the upgrade of the secondary air pump, needed to increase the air flow rate from 45 to 55 kg/h, leads to about 250 W of additional requested power, compared to the 500 W needed to switch from 2.5 kW to 3 kW of EHC power. Moreover, this solution brings benefits also in terms of DOC thermal management, since a lower heating power allows to limit the maximum temperature reached by the DOC leading to lower degradation due to poisoning and thermal ageing and higher NO conversion efficiency, as already mentioned.

Based on all these considerations, from this point on the analysis has been focused on the configurations adopting the maximum air flow rate that can be actually

provided. As it can be noticed in the lower plot of Fig. 3.9, the trend of NO_x reduction gets less and less steep as the pre-heating time increases, until getting closer to an asymptotic value. On the other hand, the CO_2 trend, shown in Fig. 3.10, is essentially monotonically increasing with the pre-heating time, due to the higher energy consumption that is compensated by an increased use of the ICE in order to keep the SoC above the lower threshold. In addition, what stands out from CO_2 trend is also an emission reduction for a limited pre-heating duration with respect to the base strategy with no pre-heating, despite the additional energy consumption requested in the first case. This is because, according to the adopted hybrid strategy described in the previous section, after the first start the ICE can be switched off again only when the DOC light-off is achieved. As a consequence, the engine is forced to run for longer if no pre-heating is planned, due to lower temperature of the EATS, and this completely deletes the advantage in terms of CO_2 reduction related to the energy saved if no pre-heating takes place. Beyond this additional consideration, according to the purpose of this activity, the pre-heating duration has been set to 100 seconds, in order to provide a result in terms of NO_x reduction that is close to the asymptotic one but that at the same time leads to a limited CO_2 increase (between 1 and 2 %). In fact, beyond this pre-heating duration the gain in terms of NO_x reduction becomes less attractive considering the related cost in terms of CO2 emission.

Concerning the heating power, for a fixed heating time in a range between 90 and 140 seconds, a considerable improvement in terms of NO_x emission can be observed by increasing the heating power from 2 kW to 2.5 kW, while no such significant advantages are introduced by further increase the heating power to 3 kW, compared to the resulting drawbacks related to a higher energy consumption and higher temperature peaks reached at the DOC. Moreover, a heating power of 2.5 kW allows to keep DOC temperature in a suitable range providing high NO conversion efficiency and almost avoiding issues related to catalyst poisoning, which take place at higher temperature (above 350-400°C).

To summarize, the maximum air flow rate available has been chosen due to the advantage introduced in terms of heating time reduction with limited increase of energy consumption and no additional raising of the temperature peaks reached by

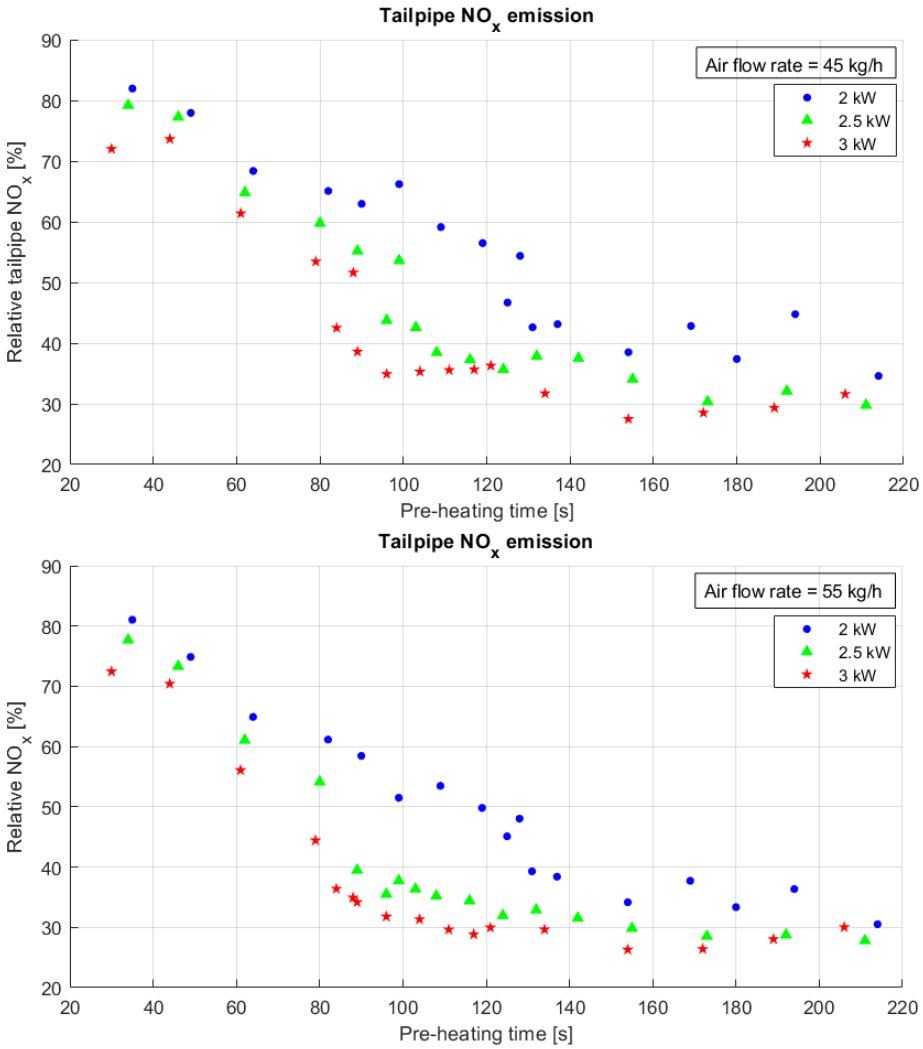

Figure 3.9: Relative tailpipe NO_x emission for variable EHC power and pre-heating time considering two different air flow rates: 45 kg/h (top) and 55 kg/h (bottom). Relative emission is calculated as the ratio between the cumulative NO_x emission [mg] resulting from the considered pre-heating strategy and the one obtained with no pre-heating along the same driving cycle.

the DOC. At the same time, the lowest EHC heating power enabling good results in terms of NO_x emission has been considered, combined with a maximized air flow rate and longer heating time in order to reach the same effects that would be reached with a higher heating power, but avoiding the aforementioned issues related to DOC thermal management. Finally, the pre-heating time has been set based on

the balance between the gain in terms of NO_x emission and the increase of CO_2 emission on the other side, due to higher energy consumption.

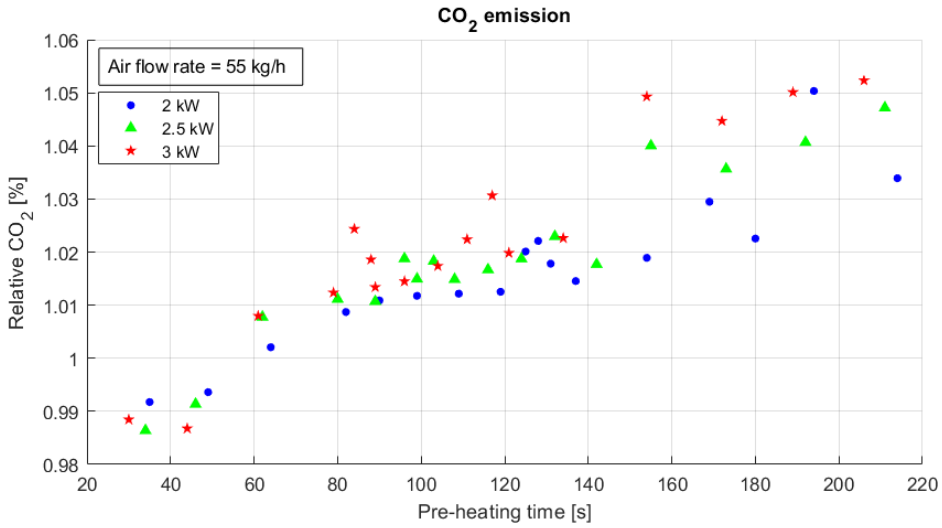

Figure 3.10: Relative CO_2 emission for variable EHC power and pre-heating time for fixed air flow rate of 55 kg/h. Relative emission is calculated as the ratio between the CO_2 emission [g/km] resulting from the considered pre-heating strategy and the one obtained with no pre-heating along the same driving cycle.

3.2.2 Development and validation of a predictive EHC control function

Backward vehicle model

As anticipated, the prediction of engine first start is the key enabler for the development of the described EHC predictive control strategy. In this regard, a simplified and thus faster backward vehicle model has been implemented in the HCU, allowing to estimate the trend of all the relevant quantities, with particular reference to EM torque request and HV battery SoC, from which engine start request can be derived based on the conditions for e-drive/hybrid drive selection, already discussed in the previous section concerning the adopted rule-based hybrid strategy. Besides the initial state of all the involved physical quantities, the two main input for the backward vehicle model are speed and slope profiles along the selected route, allowing to calculate the total requested torque at the wheels thanks to the same

equations of vehicle dynamics already presented in chapter 2. A transmission model is also present, calculating the gear profile based on the same rule-based shifting strategy implemented in the HCU subsystem responsible for the gear shifting. Since the aim is to predict engine first start, e-drive is the only driving mode considered within the prediction, so that once known the selected gear, EM torque request can be easily derived from the total torque request. Starting from the power request, a HV battery model, similar to the one described in chapter 2, allows to calculate the SoC trend, together with battery temperature which, besides influencing the SoC itself, becomes of great interest in view of a predictive battery thermal management [27].

Considering real-world driving, while the slope profile is made available directly by the map service provider, it is not possible to know a-priori the vehicle speed profile using only map data, since the driver behaviour must be taken into consideration to predict in a realistic way the vehicle speed in each segment of the planned route. In this regard, an algorithm for the prediction of vehicle speed profile along a given route, based on the elaboration of real-time navigation data, has been implemented in the HCU. In particular, information about the legal speed limits, the traffic density and the presence of the so-called "stop events", such as traffic lights and roundabouts, that in real-world driving are sent to the vehicle by the map service provider, constitute the input for the algorithm. Then, according to the vehicle performance parameters and the chosen driver behaviour, that can go from quiet to aggressive, the prediction of acceleration and braking phases is generated. Finally, as anticipated, the derived vehicle speed profile constitutes an input for all the predictive control functions that can be implemented on the vehicle. All the details about the development, implementation and validation of the speed profile prediction algorithm can be found in [28].

Since the reconstruction of vehicle speed profile is beyond the target of this activity, eHorizon provider and map database have not been implemented in the simulation environment and the same speed profile that the driver model will follow is given as input to the backward vehicle model, which in real-world driving would mean to assume that the speed profile prediction is correct.

Engine start prediction

As already introduced in the previous paragraph, the prediction of vehicle speed profile, engine torque request and SoC trend, coming from the backward vehicle model, will be the input for a dedicated function that has been developed and introduced in the HCU model in order to predict engine first start. More in detail, the output of this function will be the time instant in which the engine start is expected to be requested, namely when at least one of the following conditions is true:

- Predicted vehicle speed above 140 km/h;
- Predicted EM torque request beyond the continuous torque available at the considered speed;
- Predicted SoC lower than 18 %.

All the mentioned thresholds have been already discussed in the section describing the adopted torque split strategy.

It must be underlined that the so obtained engine start prediction does not take into account the additional energy consumption coming from EHC and secondary air pump during the EATS pre-heating phase. This is because the pre-heating phase is planned subsequently to the ICE start prediction itself. Due to this, a significant error is introduced in the SoC trend prediction, that becomes actually a problem if ICE start is driven by the condition related to low SoC, leading to an error on the engine start prediction that can not be neglected for the purposes of this activity. For this reason, a later correction must be applied to the prediction in order to overcome this issue. To do that, the additional energy ΔE needed to perform the pre-heating phase is calculated based on the requested power P_{EHC} and heating time ΔT_{heat} that have been previously set:

$$\Delta E = P_{EHC} \cdot \Delta T_{heat} \tag{3.1}$$

This amount of energy is then subtracted to the total energy provided by the HV battery to identify the correct time instant in which the SoC will drop below the

selected threshold determining the ICE start request.

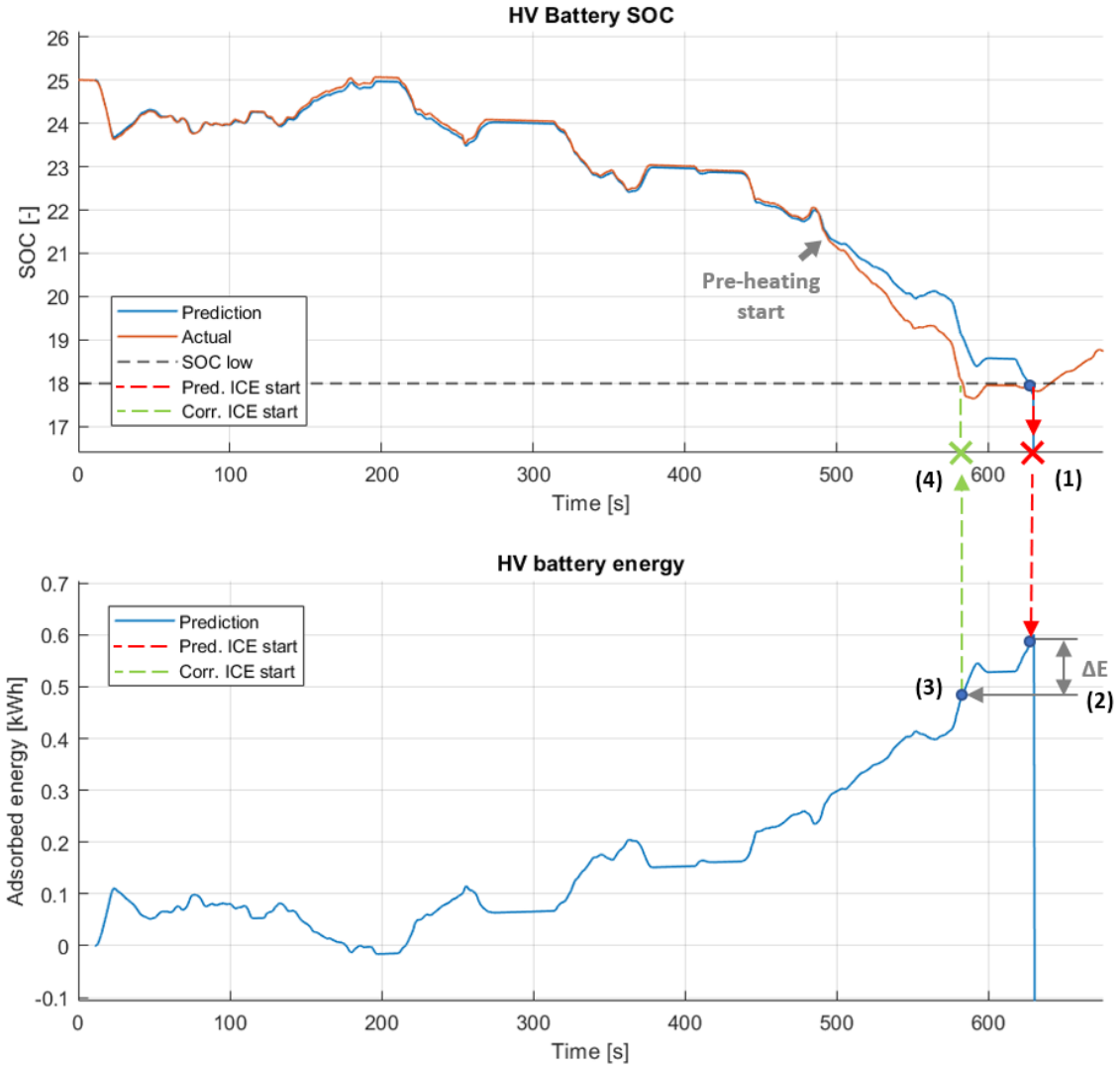

Figure 3.11: Predicted and actual HV battery state of charge (top) and corresponding adsorbed energy (bottom) along an RDE urban cycle with 25% initial SoC. According to the adopted convention, a positive gradient in the energy curve corresponds to battery discharging, while a negative gradient to battery charging.

For the sake of clarity, the plot on the top of Fig. 3.11 shows a comparison between the predicted SoC trace (not corrected) and the actual one along the first part of an RDE urban cycle starting with very low SoC. As it can be seen, in the first

500 seconds of the cycle the two traces are almost coincident except for a slight offset due to natural inaccuracies of the predictive model. Then a significant deviation between the two trends can be noticed when the pre-heating phase starts, based on the prediction itself. The additional energy request leads to a faster decrease of the actual SoC, thus causing the actual ICE start to happen in advance with respect to the prediction. As a consequence, if a correction is not applied, this would lead to a shorter heating phase with respect to the planned one. Therefore, the focus is shifted to the prediction of the energy absorbed by the HV battery, shown in the bottom of Fig. 3.11: starting from the time instant corresponding to the predicted engine start (1), the amount of energy absorbed during the pre-heating (2) is subtracted to the prediction of the total energy provided by the battery until that moment (3); finally the time instant related to the so obtained energy value corresponds to the actual ICE start if the pre-heating energy had been taken into consideration, referred to as corrected ICE start (4).

Simpler methods, like subtracting a fixed amount of energy to the HV battery in the backward vehicle model at the beginning of the prediction or raising the lower SoC threshold used for the ICE start prediction (which is equivalent to starting the prediction with a lower initial SoC), could be applied as well in order to achieve the same target. However, unlike these methods, the adopted one does not influence the prediction of battery SoC for the following part of the driving cycle, which could introduce significant errors in the ICE start prediction.

The effectiveness of the performed correction is tested over different driving cycles starting with different initial SoC as well. Only the cases in which ICE start request is determined by the condition related to low SoC are considered, since, of course, only in this situation the described correction needs to be applied. The results, summarized in Tab. 3.3, prove that in most cases the introduced correction allows to reduce significantly the gap between predicted and actual engine start, which was the main target, even if a residual error is still present due to inevitable inaccuracies of the simplified backward model implemented in the HCU. Generally, the level of accuracy achieved is enough for the purposes of this application.

Finally, the output signal carrying the information about the time instant corresponding to the predicted engine start, which is calculated by the HCU in the

Table 3.3: ICE start prediction testing over different driving cycles and initial HV battery SoC.

Cycle	Initial SoC [%]	Predicted ICE start [s]	Corrected ICE start [s]	Actual ICE start [s]
WLTC	22	502	452	453
	25	617	672	675
	30	1416	1347	1350
RDE	22	279	251	256
	25	636	599	608
	30	855	839	847
TFL	22	1003	916	917
	25	1401	1341	1324
	30	2024	1956	1958

first few seconds of driving, is sent to the engine controller, which is responsible for the management of the EHC and the secondary air pump as well. Based on this information, the pre-heating phase is planned using a timer, according to the pre-heating time that has been set. The pre-heating phase automatically stops when the engine is switched on and from that moment the EHC is managed according to the previously described rule-based strategy.

The significant gain achieved in terms of NO_x emission reduction by introducing an EHC predictive control function is widely presented in chapter 4.

Chapter 4

Simulation and results

In this chapter, firstly the gain in terms of NO_x emission reduction obtained by introducing an EHC managed with a simple rule-based strategy will be presented and discussed. Then, the improvement provided by the implementation of a predictive EHC control strategy will be highlighted by comparing the results obtained with the two different strategies. The last step will be to convert part of the gain in terms of NO_x emission reduction into a cost saving resulting from a vehicle decontenting process.

4.1 Test cases and conditions

As a first step, in order to evaluate the advantages provided by the introduction of the EHC, a set of simulations representative of the currently in-force regulation have been performed. In particular CO_2 and NO_x emissions are evaluated according to WLTP and RDE test procedures. Then, different real driving scenarios have been considered to highlight the advantages introduced by the implementation of a predictive EHC control strategy with respect to the rule-based one. The same ambient temperature, set to 25°C, has been considered for all the test cases due to the lack of data related to EATS conversion efficiency for lower temperatures. Therefore the effect of variable environmental conditions on the resulting CO_2 and NO_x emission will be not investigated within this work.

4.1.1 In-force regulation

As anticipated, the standard vehicle homologation procedure for PHEVs will be considered to effectively quantify the NO_x emission reduction that could be achieved thanks to the introduction of the EHC in the exhaust line. In this regard, firstly a complete WLTP standard procedure has been simulated according to the guidelines provided by the Regulation No 2017/1151 [23]. The resulting weighted CO_2 emission and average NO_x emission over the reference CS cycle are evaluated before and after the introduction of the EHC.

Then, a more demanding RDE test procedure, already introduced in chapter 1, has been considered to evaluate real-driving NO_x emissions. More in detail, according to PHEVs regulation, two separate tests must be performed and thus simulated:

- **Charge Depleting (CD) test** A complete RDE cycle is performed in CD mode and cumulative NO_x emissions m_t [mg] are evaluated along the complete trip. Then the distance-specific mass emission $M_{t,CD}$ [mg/km] is calculated as:

$$M_{t,CD} = \frac{m_t}{d_{t,RDE}} \tag{4.1}$$

  where $d_{t,RDE}$ is the overall travelled route;

- **Charge Sustaining (CS) test** A complete RDE cycle is performed in CS mode. The total pollutant emissions [mg] are evaluated both for complete trip (m_t) and over the urban part of the trip (m_u). The total mass of CO_2 [g] emitted over the complete RDE trip ($m_{t,CO2}$) and over the urban part of the trip ($m_{u,CO2}$) is calculated; then the distance-specific mass of CO_2 [g/km] emitted over the WLTC in CS mode ($M_{WLTC,CO2}$) is determined, in order to calculate the distance-specific mass emissions $M_{t,CS}$ and $M_{u,CS}$ [mg/km] for the complete RDE and urban part of the trip respectively:

$$M_{t,CS} = \frac{m_t}{m_{t,CO_2}} \cdot M_{WLTC,CO_2} \tag{4.2}$$

$$M_{u,CS} = \frac{m_u}{m_{u,CO_2}} \cdot M_{WLTC,CO_2} \tag{4.3}$$

More details, including the vehicle requirements, the verification of the validity of

the trip and the normality of test conditions are indicated in the relevant regulation [8].

As for the WLTP, the resulting average NO_x emissions before and after the introduction of the EHC are evaluated and compared. No predictive strategy is applied in this first set of simulations since actually not allowed by the in-force regulation.

4.1.2 Real driving scenario

In order to evaluate the potential of a predictive EHC control strategy with respect to a rule-based one, the two strategies have been tested over different driving cycles representative of real driving conditions. In particular, three urban driving cycles, listed in Tab. 4.1, have been selected in order to provide challenging conditions from the point of view of NO_x emission, being characterized by engine low load operation and frequent start and stop phases.

Table 4.1: Simulated driving cycles and relevant features. The calculated average speed does not take into account vehicle stops.

		RDE 1	**RDE 2**	**TFL**
Duration	[s]	2070	1770	2310
Distance	[m]	10510	12219	8467
Perc. stop	[%]	27	17.1	31.7
Max. speed	[km/h]	47.2	48.6	51.2
Avg. speed	[km/h]	25.0	30.0	19.3
Max. acc.	[m/s^2]	3.50	3.16	3.42

The initial battery SoC for each simulation has been varied between 22% and 30% in order to force ICE start within the driving cycle. The improvement achieved thanks the introduction of an EATS pre-heating phase based on ICE start prediction will be highlighted considering EATS components temperature profile over time and the resulting average NO_x emission along each considered cycle.

This type of test could be interesting also in view of the incoming EURO 7 regulation, which will be likely focused on the real time monitoring of pollutant emissions in nearly any possible driving scenario, promoting the development of innovative technologies and advanced control strategies to meet the more demanding pollutant targets. In this context, a comparison with the EURO 7 NO_x estimated emission limits will be provided, highlighting the key role that predictive control strategies would play in order to be compliant with such restrictions.

4.2 Results

4.2.1 WLTP test procedure

The results obtained considering a complete WLTP procedure performed with and without EHC are summarized in Tab. 4.2. A significant reduction of average NO_x emission on the CS reference cycle can be noticed thanks to the introduction of the EHC, while the resulting fuel consumption (FC), and thus CO_2 emission, evaluated on the combined cycle is basically the same. Fig. 4.1 - 4.4 show the trends of the most relevant quantities over the reference WLTC performed in CS mode. In particular, as clarified by Fig. 4.4, after the first ICE start a faster heating-up of the SCR catalyst can be achieved thanks to the EHC, thus resulting in higher NO_x conversion efficiency and lower tailpipe emission for the same ICE operating conditions.

Table 4.2: WLTP test procedure: comparison between EATS layouts with and without EHC.

		w/o EHC	**w/ EHC**	**Gain [%]**
FC CD	[l/km]	0.6	0.6	0
FC CS	[l/km]	6.8	6.8	0
FC comb.	[l/km]	2.3	2.2	-4.3
CO_2 CD	[g/km]	15.5	15.8	+1.9
CO_2 CS	[g/km]	179.5	178.1	-0.8
CO_2 comb.	[g/km]	59.1	58.9	-0.3
Avg. NO_x	[mg/km]	20.5	12.6	-38.5

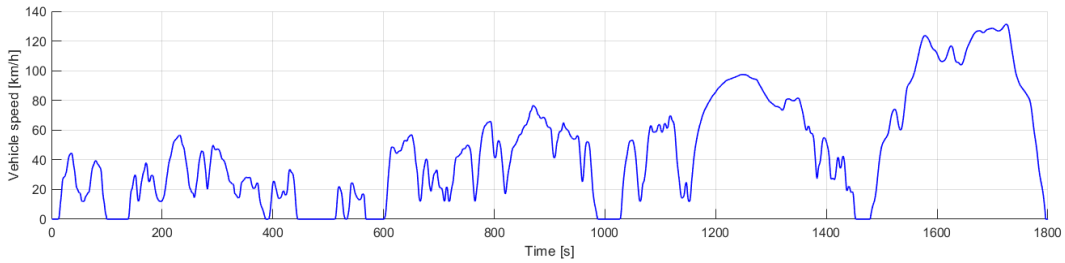

Figure 4.1: WLTP test procedure: driving cycle vehicle speed profile (null slope).

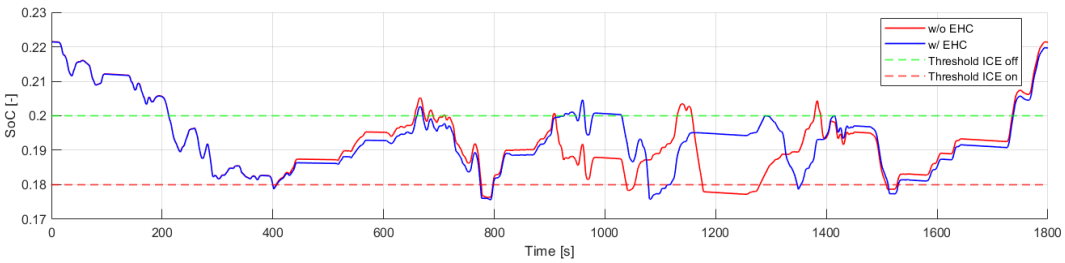

Figure 4.2: WLTP test procedure: comparison of SoC traces before and after EHC introduction over the CS reference cycle.

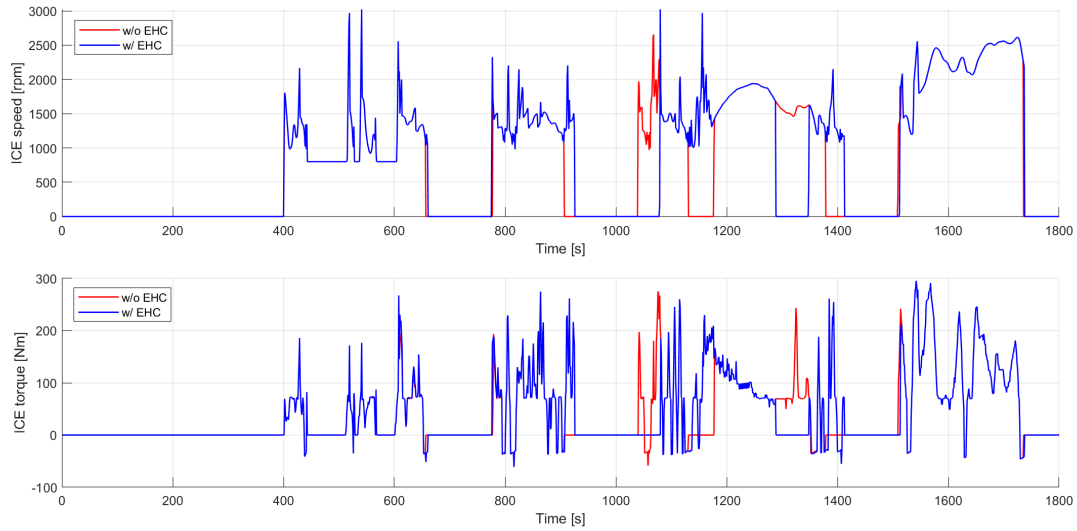

Figure 4.3: WLTP test procedure: comparison of ICE speed (top) and torque (bottom) before (red) and after (blue) EHC introduction over the CS reference cycle.

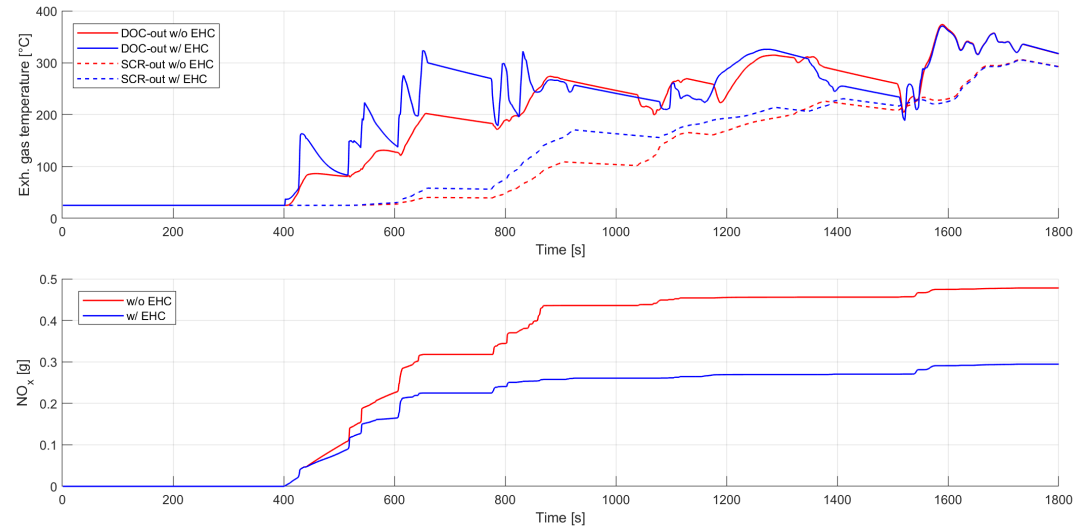

Figure 4.4: WLTP test procedure: comparison of exhaust gas temperature at DOC and SCR outlet (bottom) and resulting NO_x tailpipe emission before (red) and after (blue) EHC introduction over the CS reference cycle.

4.2.2 RDE test procedure

The results obtained considering an RDE standard test procedure performed with and without EHC are summarized in Tab. 4.3. Vehicle speed profile and road slope of the specific RDE cycle that has been considered for the test are shown in Fig. 4.5. As for the previous WLTP procedure, no significant variation of the resulting CO_2 emission are observed. A reduction of average NO_x emission can be noticed with the introduction of the EHC for all the test cases, being of course more significant for the CS cycles due to a larger use of the engine. In absolute terms, the most demanding situation in terms of NO_x emission is the RDE urban cycle performed in CS mode: ICE is repeatedly forced on due to low SoC and EATS conversion efficiency is very low due to the cold start and ICE low load operation. The trends shown in Fig. 4.6 - 4.11 refer to this specific part of the test procedure.

Table 4.3: RDE test procedure: comparison between EATS layouts with and without EHC.

			w/o EHC	**w/ EHC**	**Gain [%]**
RDE CD	CO_2	[g/km]	101	100	-1.0
	NO_x	[mg/km]	18.8	17.1	-9.0
RDE CS	CO_2	[g/km]	174	176	+1.1
	NO_x	[mg/km]	15.2	9.9	-34.9
RDE urban CS	CO_2	[g/km]	252	247	-2.0
	NO_x	[mg/km]	31.0	18.6	40.0

More in detail, thanks to the introduction of the EHC, the DOC light-off temperature can be achieved in a shorter time, as shown in Fig. 4.8; this allows an earlier switch from hybrid to e-drive with respect to the case with no electrical heating, namely as soon as the SoC-related condition is fulfilled (4.7), according to the adopted torque split strategy described in chapter 3. Fig. 4.8 shows also the resulting NO_2/NO_x ratio, which is generally higher in the case with EHC thanks to the higher DOC temperature.

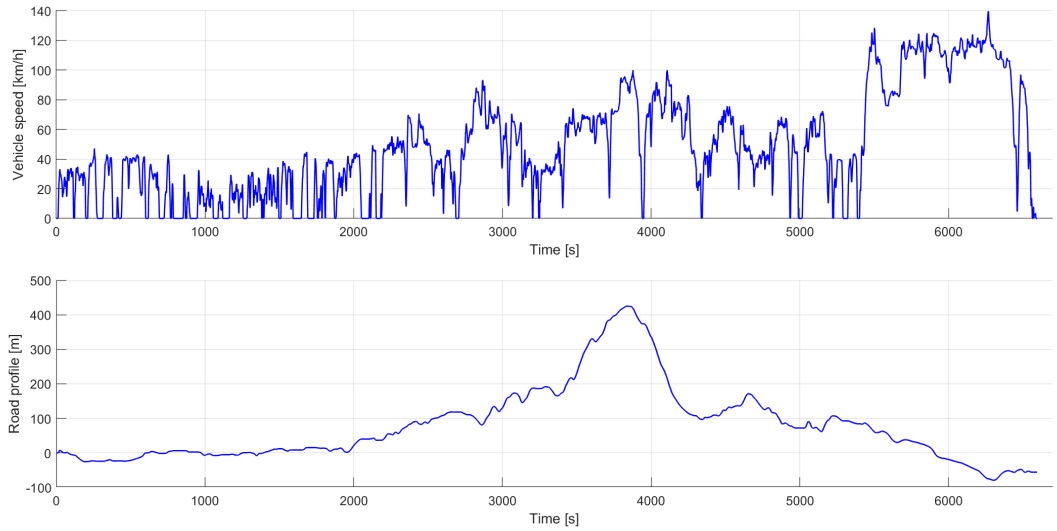

Figure 4.5: RDE test procedure: driving cycle speed (top) and slope (bottom) profiles.

The advantage achieved by introducing the EHC is even clearer looking to LTM-SCR and SCR temperature profiles and the corresponding injected AdBlue, shown in Fig. 4.9 and 4.10 respectively: the faster LTM-SCR heating phase provided by the EHC allows to reach the temperature threshold to activate AdBlue injection in a shorter time; concerning the SCR, the mentioned temperature threshold is not even reached within the driving cycle without EHC intervention, thus resulting in no additional injected urea apart from the limited quantity already stored in the device. As expected, all these considerations converge into a reduction of cumulative tailpipe NO_x emission along the considered driving cycle thanks to EHC introduction (Fig. 4.11).

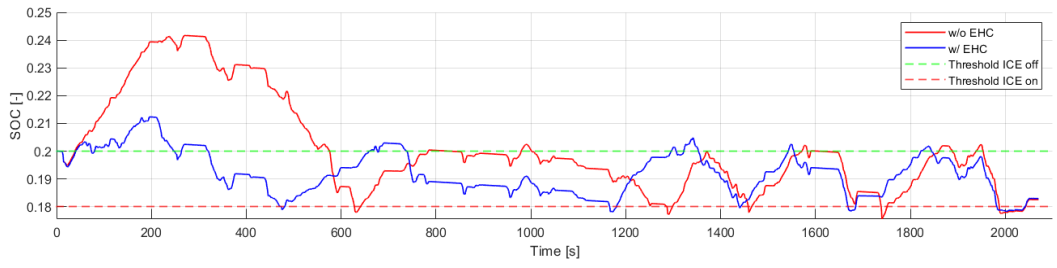

Figure 4.6: RDE test procedure: comparison of SoC traces before (red) and after (blue) EHC introduction over the urban part of the cycle in CS mode.

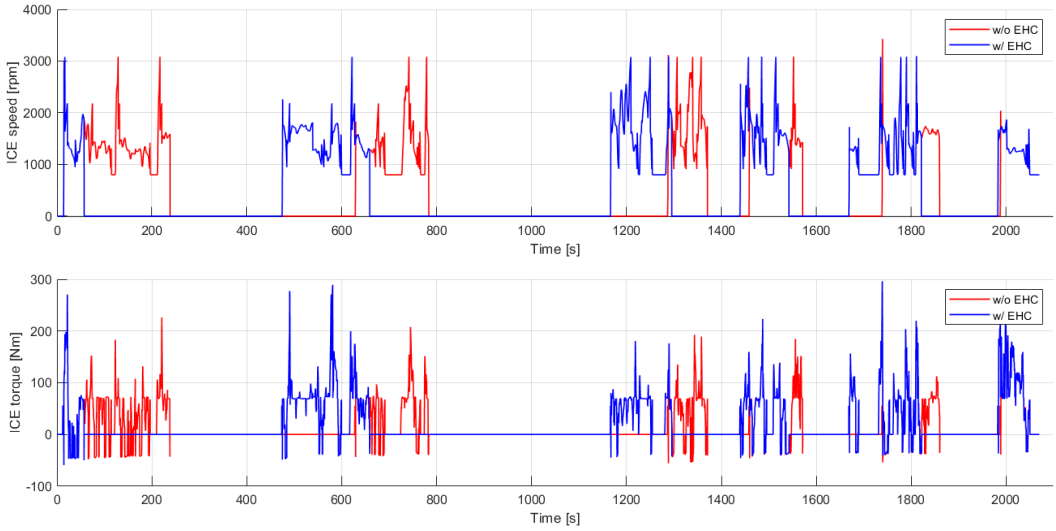

Figure 4.7: RDE test procedure: comparison of ICE speed (top) and torque (bottom) before (red) and after (blue) EHC introduction over the urban part of the cycle in CS mode.

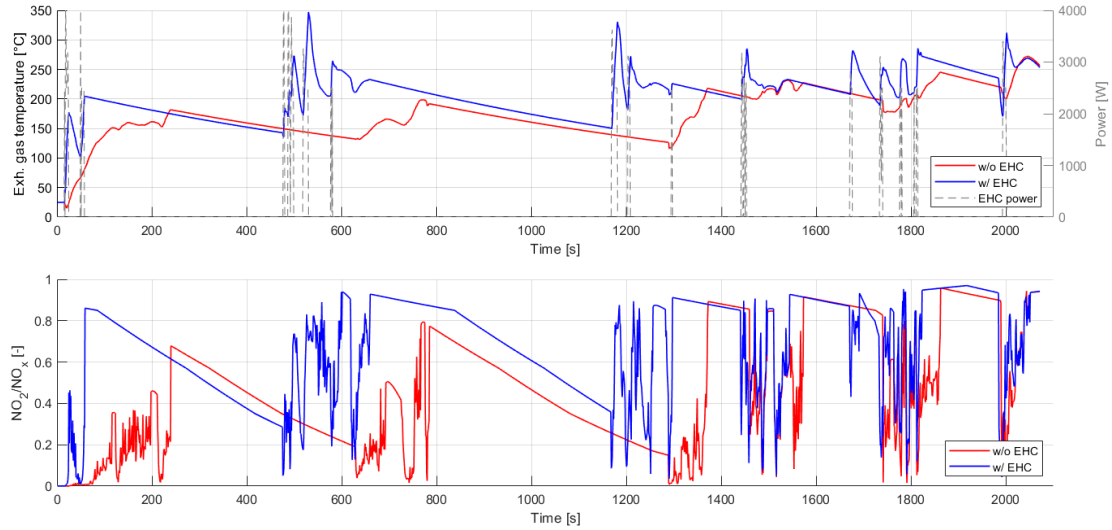

Figure 4.8: RDE test procedure: comparison of DOC-out exhaust temperature (top) and resulting NO_2/NO_x ratio (bottom) before (red) and after (blue) EHC introduction over the urban part of the cycle in CS mode.

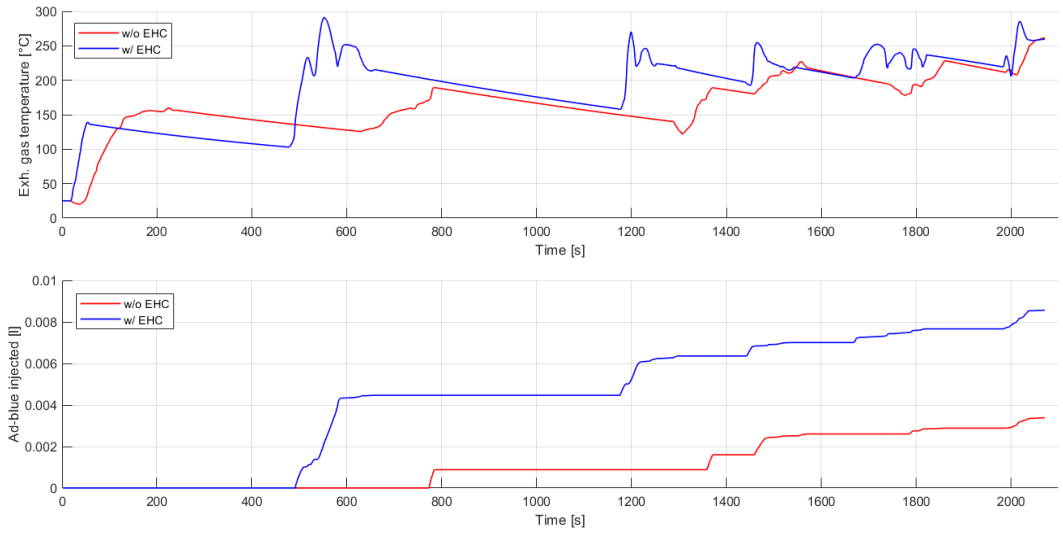

Figure 4.9: RDE test procedure: comparison of LTM-SCR-out exhaust temperature (top) and resulting injected AdBlue (bottom) before (red) and after (blue) EHC introduction over the urban part of the cycle in CS mode.

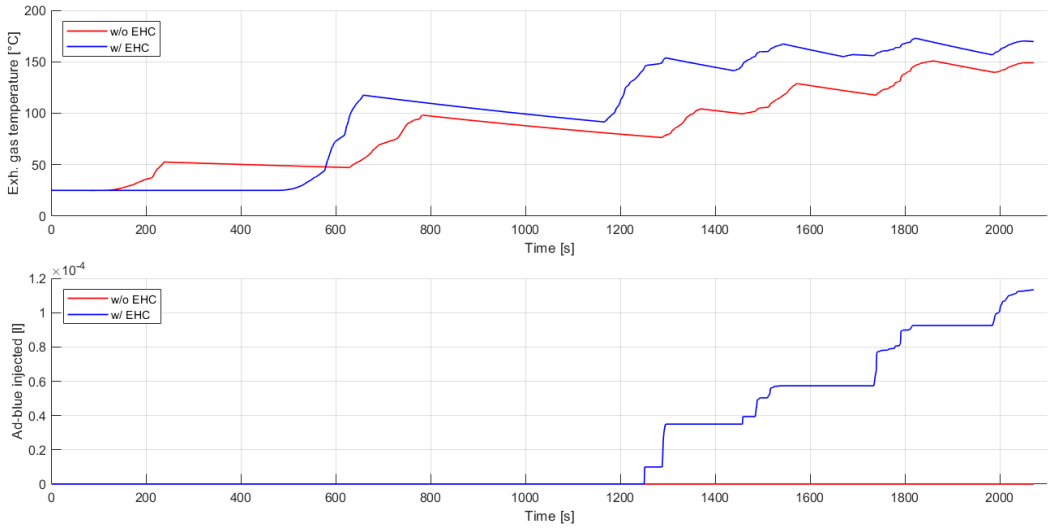

Figure 4.10: RDE test procedure: comparison of SCR-out exhaust temperature (top) and resulting injected AdBlue (bottom) before (red) and after (blue) EHC introduction over the urban part of the cycle in CS mode.

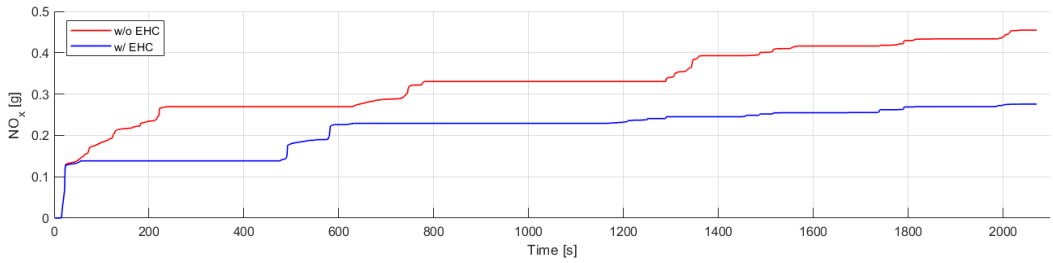

Figure 4.11: RDE test procedure: comparison of cumulated tailpipe NO_x emission before (red) and after (blue) EHC introduction over the urban part of the cycle in CS mode.

4.2.3 Real driving scenarios

The results in terms of NO_x and CO_2 emissions along the three considered urban driving cycles for different initial SoC are summarized in Tab. 4.4. In particular, a comparison between rule based and predictive EHC control strategies is provided. Vehicle speed profile and road slope of the considered driving cycles are shown in Fig. 4.12 - 4.14.

The overall CO_2 trend is slightly increasing switching from the rule-based strategy to the predictive one, which includes an EATS pre-heating phase and thus significant additional energy consumption. A significant reduction of average NO_x emission is achieved with the implementation of a predictive strategy in most of the cases.

Three cases among those simulated are deeper analysed in the following paragraphs as representative of possible different situations that can be encountered, based on all the observed cases:

- **Case 1** RDE 1 urban cycle with 25% initial SoC;
- **Case 2** TFL urban cycle with 25% initial SoC;
- **Case 3** TFL urban cycle with 30% initial SoC.

Table 4.4: Comparison between predictive (PS) and rule-based (RBS) EHC control strategies: resulting CO_2 and NO_x emission over different urban driving cycles with variable initial SoC.

	Init. SoC [%]	**NO_x** [mg/km]			**CO_2** [g/km]		
		w/o EHC	EHC RBS	EHC PS	NO EHC	EHC RBS	EHC PS
RDE 1	22	34.6	17.9	5.8	228	233	240
	25	38.4	20.3	7.6	205	198	222
	30	35.0	14.7	5.0	124	132	143
RDE 2	22	20.0	8.8	2.5	190	188	195
	25	24.0	11.6	6.2	162	158	170
	30	31.4	11.5	2.9	99.6	103	114
TFL	22	44.3	18.7	16.7	205	213	214
	25	47.3	20.5	16.9	160	166	171
	30	31.2	32.5	2.6	58.6	66.8	61.2

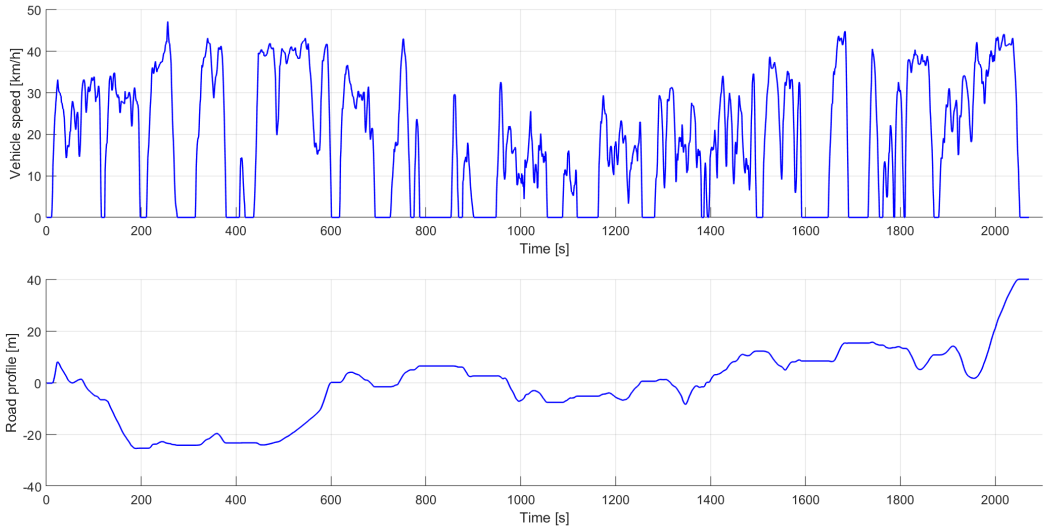

Figure 4.12: RDE 1 urban cycle: driving cycle speed (top) and slope (bottom) profiles.

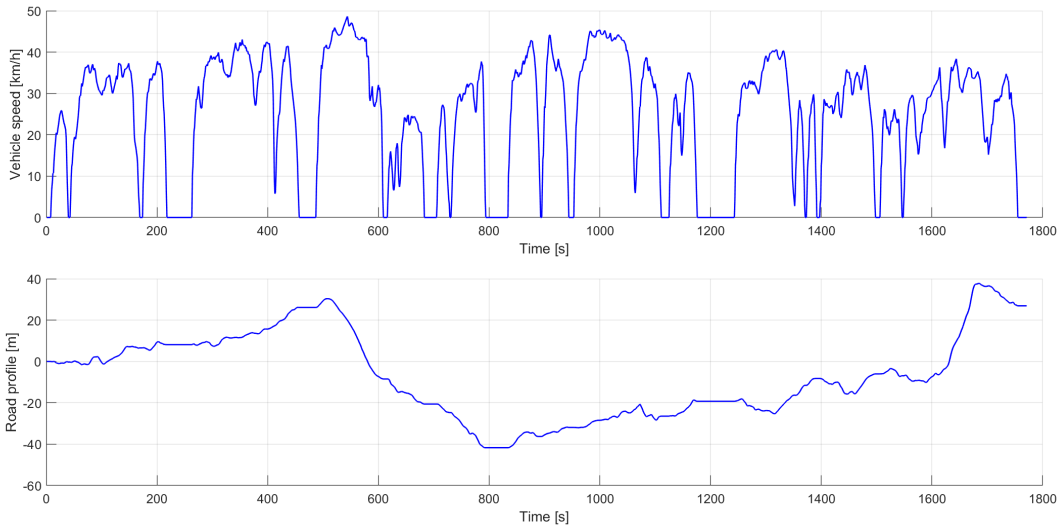

Figure 4.13: RDE 2 urban cycle: driving cycle speed (top) and slope (bottom) profiles.

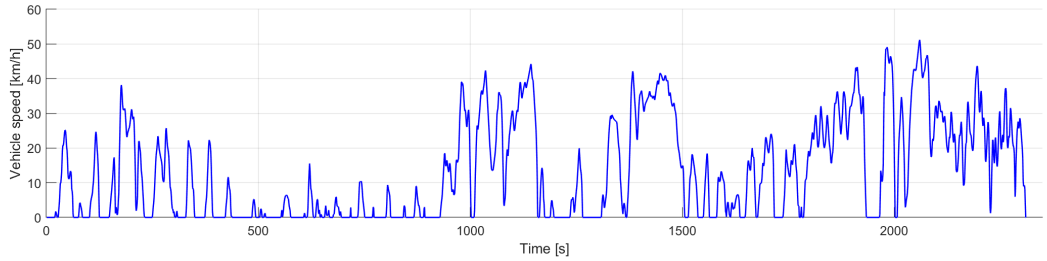

Figure 4.14: TFL urban cycle: driving cycle speed profile (null slope).

Case 1

In this case the first ICE start is determined by the SoC-related condition and it is correctly predicted by the HCU, allowing to perform the planned pre-heating phase (Fig. 4.15 - 4.16). The exhaust gas temperature profiles at DOC, LTM-SCR and SCR outlet obtained with the two different strategies are shown in Fig. 4.17, together with EHC requested power. Focusing on Fig. 4.18, it can be noticed that almost 70% of the total NO_x are emitted within the 200 seconds after the first ICE start. Therefore, the gain obtained with the introduction of a pre-heating phase is significant, allowing to heat-up in advance the two SCR catalysts and reduce the average NO_x emission along the driving cycle of more than 60%. Similar results are

obtained from the simulations on the same driving cycles with different initial SoC and also on RDE 2 driving cycle, for which the same considerations may be applied.

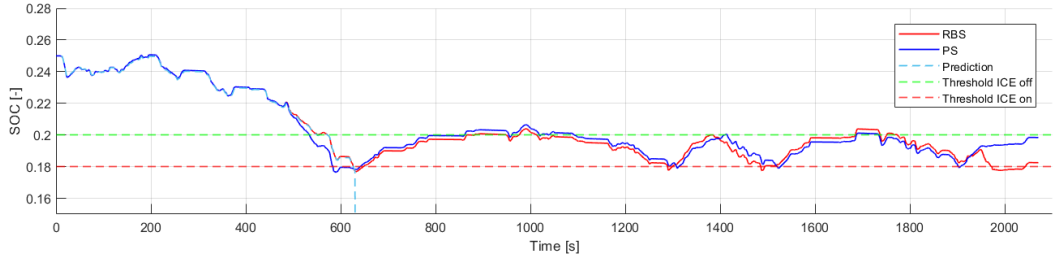

Figure 4.15: Case 1: comparison of SoC traces for rule-based (red) and predictive (blue) EHC control strategies; cyan dashed line shows the SoC trace prediction.

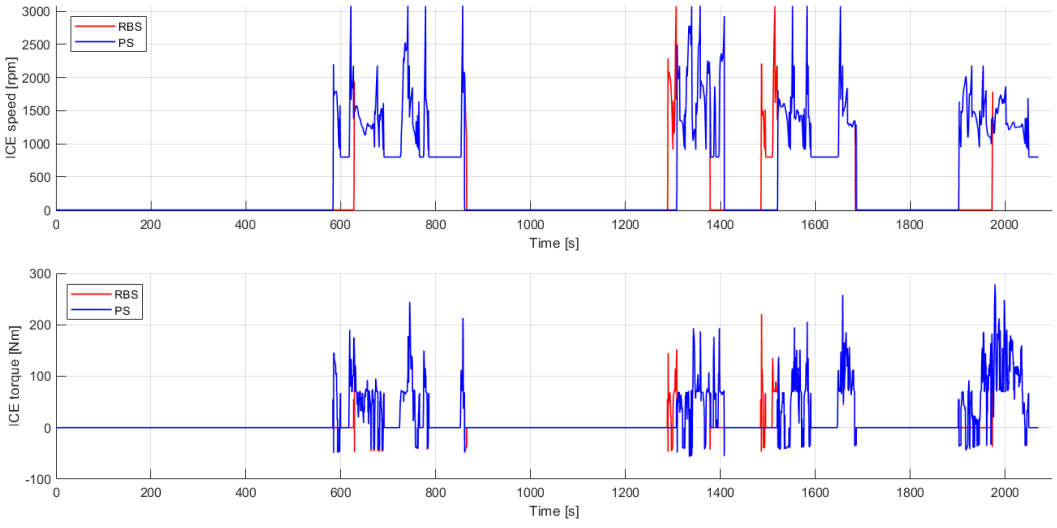

Figure 4.16: Case 1: comparison of ICE speed (top) and torque (bottom) for rule-based (red) and predictive (blue) EHC control strategies.

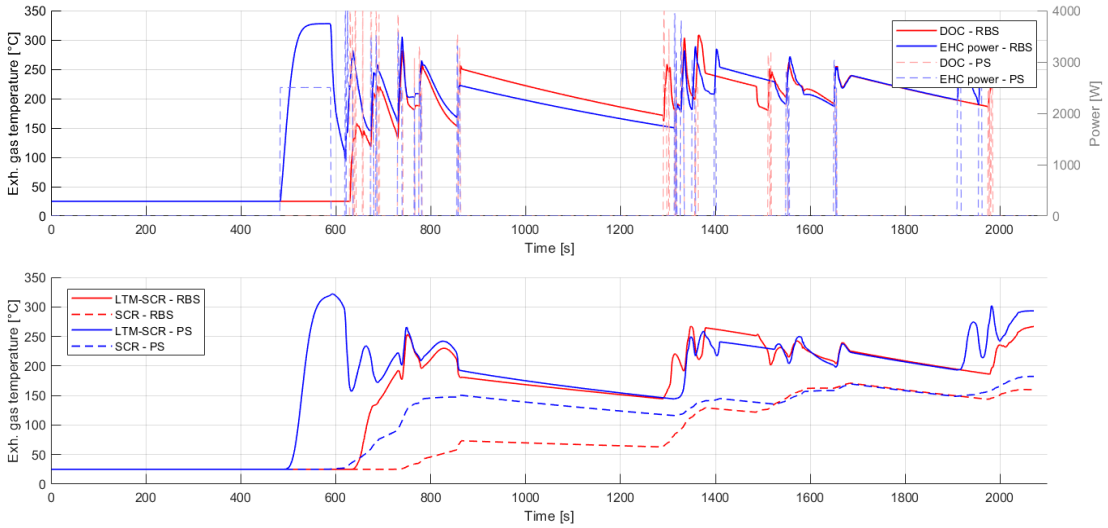

Figure 4.17: Case 1: on the top, a comparison of exhaust temperature at DOC outlet for rule-based (solid red) and predictive (solid blue) EHC control strategies and corresponding EHC adsorbed power (dashed); on the bottom, exhaust temperature at LTM-SCR (solid) and SCR (dashed) outlet for rule-based (red) and predictive (blue) EHC control strategies.

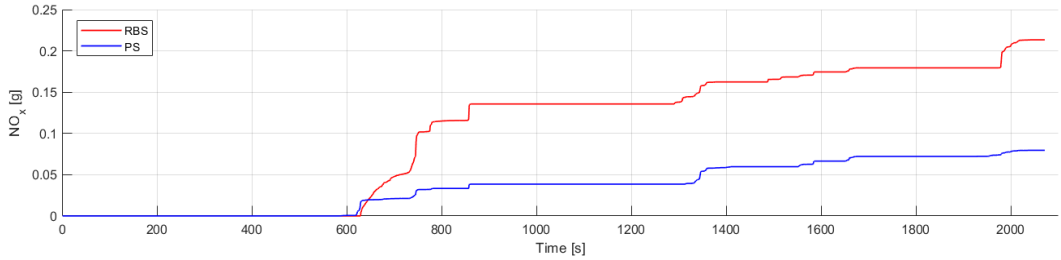

Figure 4.18: Case 1: comparison of cumulated tailpipe NO_x emission for rule-based (red) and predictive (blue) EHC control strategies.

Case 2

As for case 1, the first ICE start is determined by the SoC-related condition and it is correctly predicted by the HCU, as shown in Fig. 4.19. The exhaust gas temperature profiles at DOC, LTM-SCR and SCR outlet obtained with the two different strategies are shown in Fig. 4.21, together with EHC requested power. Despite the pre-heating phase, a higher NO_x emission is observed for the predictive strategy during the first ICE start: in this case, immediately after ICE start, there is accidentally a peak in the driver torque request. As shown in Fig. 4.22, this results in a peak of engine-out NO_x emission and therefore higher tailpipe emission with respect to the case in which the rule-based strategy is applied, despite the higher SCRs temperature and thus conversion efficiency provided by the EHC predictive strategy. Anyway, the pre-heating phase, thanks to the higher temperature reached by the SCR, allows to limit NO_x tailpipe emission for the last part of the cycle, thus compensating the higher emission resulting from the first ICE start. As a consequence, the average NO_x emission along the whole driving cycle results still a bit lower for the predictive approach, showing the effectiveness of this strategy in limiting the final tailpipe emissions, despite the much more demanding situations that may be realistically encountered. Similar considerations may be applied to the test case performed on the same driving cycle but with 22% initial SoC.

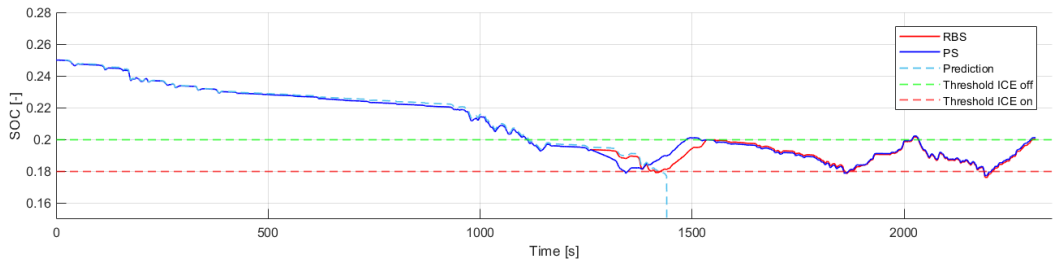

Figure 4.19: Case 2: comparison of SoC traces for rule-based (red) and predictive (blue) EHC control strategies; cyan dashed line shows the SoC trace prediction.

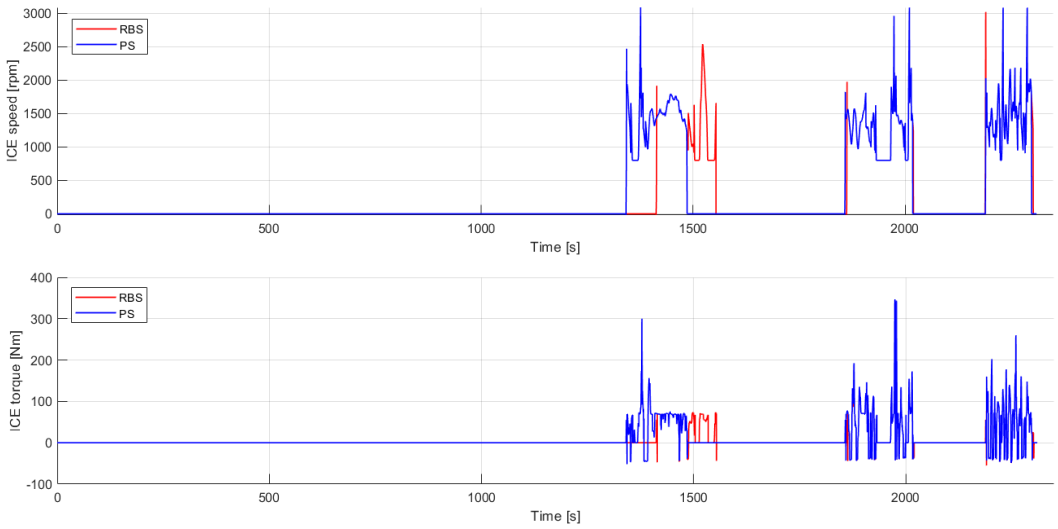

Figure 4.20: Case 2: comparison of ICE speed (top) and torque (bottom) for rule-based (red) and predictive (blue) EHC control strategies.

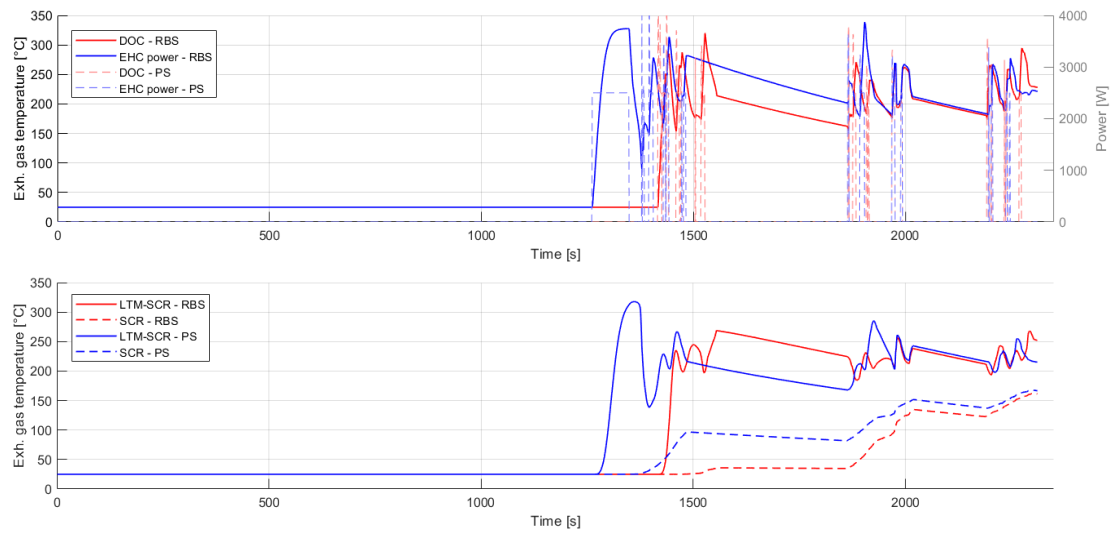

Figure 4.21: Case 2: on the top, a comparison of exhaust temperature at DOC outlet for rule-based (solid red) and predictive (solid blue) EHC control strategies and corresponding EHC adsorbed power (dashed); on the bottom, exhaust temperature at LTM-SCR (solid) and SCR (dashed) outlet for rule-based (red) and predictive (blue) EHC control strategies.

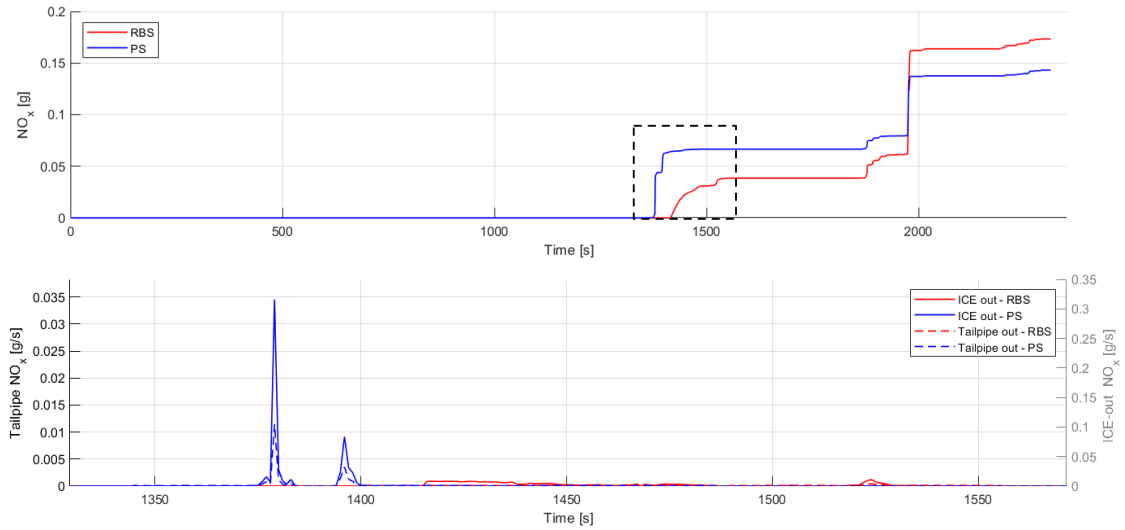

Figure 4.22: Case 2: on the top, comparison of cumulated tailpipe NO_x emission for rule-based (red) and predictive (blue) EHC control strategies; on the bottom, the corresponding instant NO_x emissions focused on ICE first start.

Case 3

In this case the first ICE start is determined by the condition related to EM torque limit and it is correctly predicted by the HCU, as proven by Fig. 4.24, which compares the actual and predicted trend of EM torque request together with the corresponding EM torque limits. The higher temperature reached by the EATS thanks to the planned pre-heating phase (4.26) allows to strongly reduce NO_x emissions due to ICE first start, as shown in Fig. 4.27. Moreover, due to the different SoC trends resulting from the two strategies (Fig. 4.23), in the case of the predictive strategy the engine keeps running for a longer time after the first ICE start with respect to the rule-based strategy and no further ICE start takes place until the and of the driving cycle. On the contrary, considering the rule-based strategy, the ICE is switched off after a few tens of seconds according to the SoC-related condition and then a second engine start is requested thus strongly increasing the total NO_x tailpipe emission due to EATS low temperature. Together with the gain introduced by the pre-heating, this fully explains the very significant reduction of average tailpipe NO_x emission presented in 4.4 for the considered test case.

To summarize, the contribution of the only predictive control strategy on the reduction of average tailpipe NO_x emission stands around the 60%. Concerning the foreseen future limits that will be introduced by the incoming EURO 7 regulation [32], the described EATS equipped with an EHC would be able to meet NO_x emission target for LCVs even without the introduction of a predictive strategy if the less demanding "Scenario A" is considered, which will set the actual limit to 30 mg/km. Nevertheless, the improvement in NO_x emission control enabled by a predictive EHC control function would be mandatory if this limit were lowered to 10 mg/km, according to the most stringent situation referred to as "Scenario B".

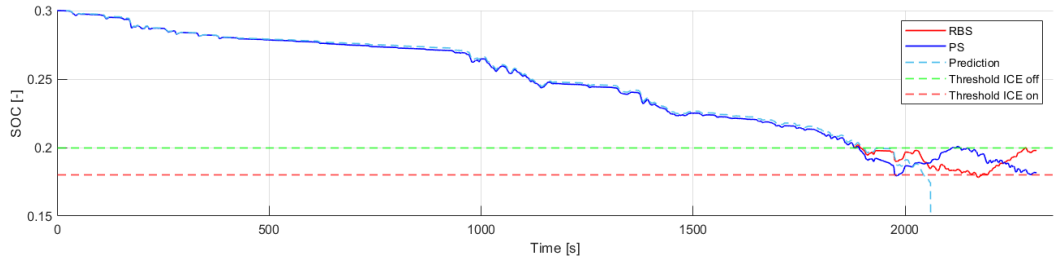

Figure 4.23: Case 3: comparison of SoC traces for rule-based (red) and predictive (blue) EHC control strategies; cyan dashed line shows the SoC trace prediction.

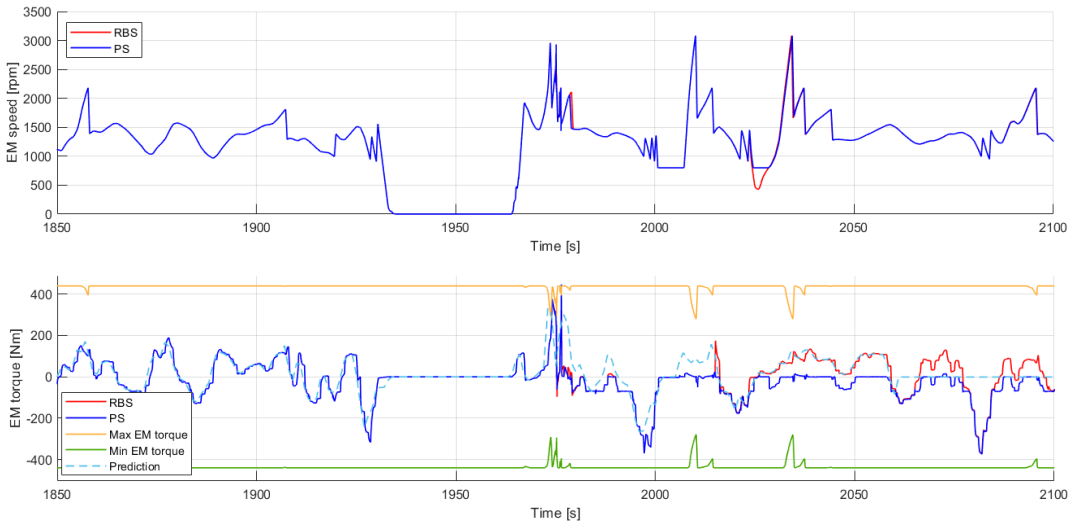

Figure 4.24: Case 3: comparison of EM speed (top) and torque (bottom) for rule-based (red) and predictive (blue) EHC control strategies; cyan dashed line shows EM torque prediction.

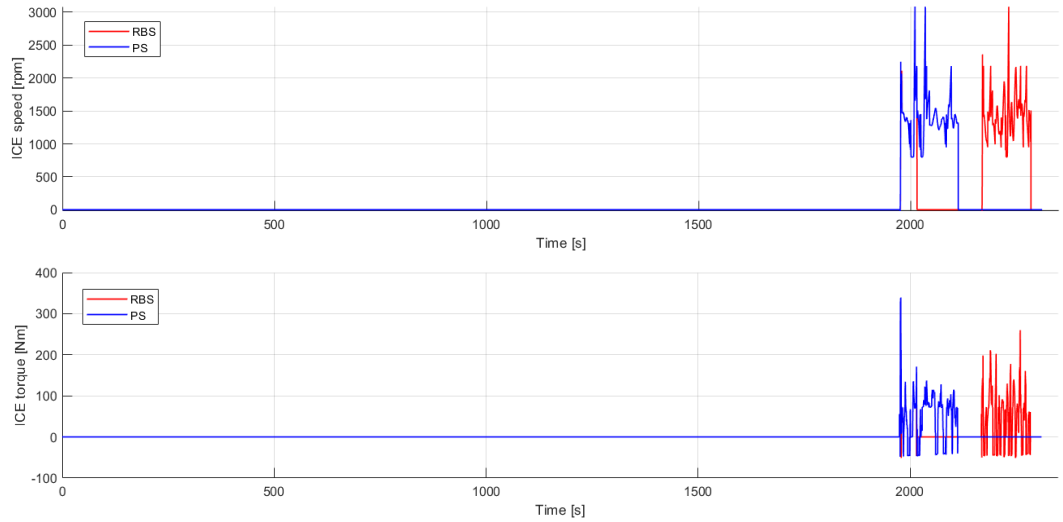

Figure 4.25: Case 3: comparison of ICE speed (top) and torque (bottom) for rule-based (red) and predictive (blue) EHC control strategies.

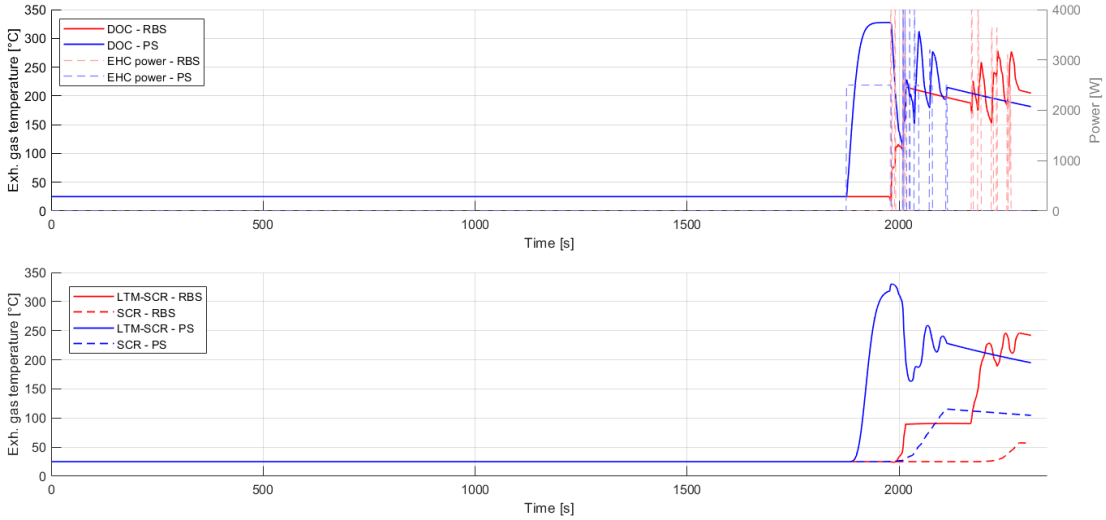

Figure 4.26: Case 3: on the top, a comparison of exhaust temperature at DOC outlet for rule-based (solid red) and predictive (solid blue) EHC control strategies and corresponding EHC adsorbed power (dashed); on the bottom, exhaust temperature at LTM-SCR (solid) and SCR (dashed) outlet for rule-based (red) and predictive (blue) EHC control strategies.

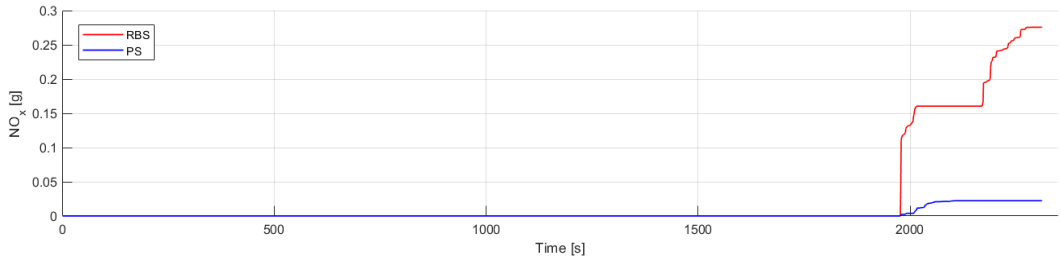

Figure 4.27: Case 3: comparison of cumulated tailpipe NO_x emission for rule-based (red) and predictive (blue) EHC control strategies.

4.3 Vehicle decontenting

Considering the less demanding EURO 7 scenario introduced in the last section, the significant margin between the very low NO_x emissions obtained implementing an EHC predictive function and the limit imposed by the regulation (30 mg/km), paves the way to a simplification of the EATS layout in order to limit the related costs.

Table 4.5: Average NO_x emission over RDE 1 urban cycle with and without LTM-SCR for rule-based and predictive control strategies.

Init. SoC [%]	**NO_x** [mg/km]				
	NO EHC	RBS	PS	RBS w/o LTM-SCR	PS w/o LTM-SCR
22	34.6	17.9	5.8	33.9	12.3
25	38.4	20.3	7.6	36.9	16.0
30	35.0	14.7	5.0	32.1	9.9

In particular, the same rule-based and predictive control strategies have been applied to a simplified EATS layout without LTM-SCR. This layout modification is completely consistent with the development of an improved EATS thermal management strategy: the introduction of an electrical heater and especially of a pre-heating phase based on engine start prediction, allow to significantly speed up the heating of all EATS devices, thus making the installation of an additional SCR with reduced thermal inertia less incisive from the point of view of limiting cold start tailpipe

emissions. The results presented in 4.5 show that the average NO_x emission, obtained performing the same simulations over RDE 1 urban cycle already described in the previous section, is still below the considered limit for all the test cases if the predictive EHC control strategy is considered.

Table 4.6: Estimated manufacturing costs of the components included in the considered EATS.

Component	**Volume** [l]	**Estimated cost** [$]
DOC	1.6	120
LTM-SCR	1.2	180
SDPF	4.0	400
SCR	3.5	750
Total cost		1450

Of course, the LTM-SCR removal has a positive impact on the total cost of the EATS, which has been quantified by estimating the likely cost of each aftertreatment device included in the exhaust line, according to the analysis carried out in [29]. Tab. 4.6 shows the estimated unit cost for each component depending on its volume, which is a function of engine displacement. The costs related to the urea storage system and dosing control unit are counted once and included in the SCR cost. As a final result, the vehicle decontenting process enabled by the implementation of the developed predictive EHC control strategy allows to save approximately between the 12% and 13% of the EATS total cost.

Chapter 5

Conclusion and future works

The present activity has been focused on the development of a predictive EHC control function for a diesel PHEV equipped with a EU7-oriented EATS. For this purpose, a complete *Simulink* model representative of the mentioned vehicle has been considered. As a first step, a rule-based strategy managing the torque split between ICE and EM has been developed and calibrated aiming to the best results in terms of tailpipe NO_x emission. Then a predictive EHC control function has been implemented in the HCU in order to plan an EATS pre-heating phase based on ICE first start prediction. The resulting NO_x emission reduction has been evaluated considering different driving scenarios with the same ambient conditions. As a consequence, the effect of ambient temperature variation on the final NO_x emissions has not been investigated within this work.

The results discussed in the previous chapter show the potential of the developed predictive control strategy in terms of EATS thermal management and NO_x emission reduction. In particular, the knowledge of future driving conditions has proven to be a key enabler to meet the most stringent pollutant emission limits that may be likely introduced by the incoming EURO 7 regulation. Moreover, the implementation of an improved control strategy for the EATS thermal management allows to adopt a simplified EATS layout and thus to reduce the total manufacturing cost while complying with the same emission limits imposed by the regulation.

Besides these promising conclusions, the tests described in the previous chapter

highlight that the final result may be strongly affected by the randomness of the occurring driving conditions. This issue must be solved in order to reach the robustness required in view of a real-world application of the proposed control strategy.

Based on all these considerations, the developed predictive control strategy can be definitely considered as a successful proof of concept to be used as a starting point for further improvements and future activities, which may include:

- extending the temperature range of the considered test cases in order to evaluate the gain introduced by the predictive control strategy when very low ambient temperatures are considered;
- improving the EHC rule-based strategy by introducing a more accurate control based on the actual temperature of EATS components;
- improving the developed control function in order to predict not only the first ICE start, but also the subsequent ones, which may lead to significant NO_x emissions as well, if taking place after a long engine-off time interval;
- integrating the developed control function with additional predictive control strategies focused on energy management, in order to achieve the best results in terms of efficiency and pollutant emissions;
- moving from a completely virtual environment (Model-in-the-Loop, MiL) to SiL (Software-in-the-Loop) and HiL (Hardware-in-the-Loop) simulation to perform a more robust validation and refined calibration of the developed control strategy, in order to evaluate more accurately the gain provided by the considered technologies and control strategies;
- switching from a deterministic to a probabilistic approach that would evaluate ICE start probability within each road segment composing the complete driving cycle, rather than the exact time instant in which it should happen. This would help to solve the problem related to inevitable prediction inaccuracies and resulting random errors that may affect the final result, thus improving the robustness of the developed control strategy in view of a real-world application.

Bibliography

[1] Kelvin O. Yoro and Michael O. Daramola. "Chapter 1 - CO2 emission sources, greenhouse gases, and the global warming effect". en. *Advances in Carbon Capture*. Ed. by Mohammad Reza Rahimpour, Mohammad Farsi, and Mohammad Amin Makarem. Woodhead Publishing, Jan. 2020, 3–28. ISBN: 978-0-12-819657-1. DOI: 10.1016/B978-0-12-819657-1.00001-3. URL: https://www.sciencedirect.com/science/article/pii/B9780128196571000013 (visited on 08/15/2021).

[2] Hannah Ritchie and Max Roser. "CO2 and Greenhouse Gas Emissions". *Our World in Data* (May 2020). URL: https://ourworldindata.org/co2-and-other-greenhouse-gas-emissions (visited on 08/15/2021).

[3] Tommaso Selleri, Anastasios Melas, Ameya Joshi, D. Manara, Adolfo Perujo, and Ricardo Suarez-Bertoa. "An Overview of Lean Exhaust deNOx Aftertreatment Technologies and NOx Emission Regulations in the European Union". *Catalysts* 11 (Mar. 2021), 404. DOI: 10.3390/catal11030404.

[4] Marilena Kampa and Elias Castanas. "Human health effects of air pollution". en. *Environmental Pollution*. Proceedings of the 4th International Workshop on Biomonitoring of Atmospheric Pollution (With Emphasis on Trace Elements) 151.2 (Jan. 2008), 362–367. ISSN: 0269-7491. DOI: 10.1016/j.envpol.2007.06.012. URL: https://www.sciencedirect.com/science/article/pii/S0269749107002849 (visited on 08/27/2021).

[5] *Air quality in Europe 2019 — European Environment Agency*. en. Publication. URL: https://www.eea.europa.eu/publications/air-quality-in-europe-2019 (visited on 08/27/2021).

[6] *Regulation (EU) 2019/631 of the European Parliament and of the Council of 17 April 2019 setting CO2 emission performance standards for new passenger cars and for new light commercial vehicles, and repealing Regulations (EC) No 443/2009 and (EU) No 510/2011 (Text with EEA relevance.)* en. Legislative Body: EP, CONSIL. Apr. 2019. URL: http://data.europa.eu/eli/reg/2019/631/oj/eng (visited on 08/24/2021).

[7] *Commission Regulation (EU) 2016/427 of 10 March 2016 amending Regulation (EC) No 692/2008 as regards emissions from light passenger and commercial vehicles (Euro 6) (Text with EEA relevance)*. en. Legislative Body: COM. Mar. 2016. URL: http://data.europa.eu/eli/reg/2016/427/oj/eng (visited on 08/24/2021).

[8] *Commission Regulation (EU) 2018/1832 of 5 November 2018 amending Directive 2007/46/EC of the European Parliament and of the Council, Commission Regulation (EC) No 692/2008 and Commission Regulation (EU) 2017/1151 for the purpose of improving the emission type approval tests and procedures for light passenger and commercial vehicles, including those for in-service conformity and real-driving emissions and introducing devices for monitoring the consumption of fuel and electric energy (Text with EEA relevance.)* en. Legislative Body: COM, GROW. Nov. 2018. URL: http://data.europa.eu/eli/reg/2018/1832/oj/eng (visited on 08/24/2021).

[9] Junfeng Zhao and Junmin Wang. "Integrated Model Predictive Control of Hybrid Electric Vehicles Coupled With Aftertreatment Systems". *IEEE Transactions on Vehicular Technology* 2 (Jan. 2015), 1–1. DOI: 10.1109/TVT.2015.2405918.

[10] Dhrupad Biswas, Susenjit Ghosh, Somnath Sengupta, and Siddhartha Mukhopadhyay. "A Predictive Supervisory Controller for an HEV Operating in a Zero Emission Zone". *2019 IEEE Transportation Electrification Conference and Expo (ITEC)*. ISSN: 2377-5483. June 2019, 1–6. DOI: 10.1109/ITEC.2019.8790631.

[11] V. Praveena and Leenus Martin. "A Review on Various After Treatment Techniques to Reduce NOx emissions in a CI Engine". *Journal of the Energy Institute* 91 (June 2017). DOI: 10.1016/j.joei.2017.05.010.

[12] Bin Guan, Reggie Zhan, He Lin, and Huang Zhen. "Review of state of the art technologies of selective catalytic reduction of NOx from diesel engine exhaust". *Applied Thermal Engineering* 66 (May 2014), 395–414. DOI: 10.1016/j.applthermaleng.2014.02.021.

[13] Ben Bargman, SooHyun Jang, Jan Kramer, Ihab Soliman, and Abhid Akram Abubeckar Mohamed Sahul. *Effects of Electrically Preheating Catalysts on Reducing High-Power Cold-Start Emissions*. English. SAE Technical Paper 2021-01-0572. ISSN: 0148-7191, 2688-3627. Warrendale, PA: SAE International, Apr. 2021. DOI: 10.4271/2021-01-0572. URL: https://www.sae.org/publications/technical-papers/content/2021-01-0572/ (visited on 08/24/2021).

[14] Jianbing Gao, Guohong Tian, Aldo Sorniotti, Ahu Ece Karci, and Raffaele Di Palo. "Review of thermal management of catalytic converters to decrease engine emissions during cold start and warm up". en. *Applied Thermal Engineering* 147 (Jan. 2019), 177–187. ISSN: 1359-4311. DOI: 10.1016/j.applthermaleng.2018.10.037. URL: https://www.sciencedirect.com/science/article/pii/S1359431118336081 (visited on 05/18/2021).

[15] Jianbing Gao, Guohong Tian, and Aldo Sorniotti. "On the emission reduction through the application of an electrically heated catalyst to a diesel vehicle". *Energy Science and Engineering* 7 (Sept. 2019). DOI: 10.1002/ese3.416.

[16] Johannes Hofstetter, Paul Boucharel, Frank Atzler, and Georg Wachtmeister. "Fuel Consumption and Emission Reduction for Hybrid Electric Vehicles with Electrically Heated Catalyst". English. *SAE International Journal of Advances and Current Practices in Mobility* 3.1 (June 2020). Number: 2020-37-0017, 702–714. ISSN: 2641-9637, 2641-9645. DOI: 10.4271/2020-37-0017. URL: https://www.sae.org/publications/technical-papers/content/2020-37-0017/ (visited on 08/24/2021).

[17] Gabriele Caramia, Nicolò Cavina, Davide Moro, Stefano Patassa, and Luca Solieri. "Predictive NOx emission control of a diesel-HEV for CO2 and urea consumption reduction". *AIP Conference Proceedings* 2191.1 (Dec. 2019). Publisher: American Institute of Physics, 020035. ISSN: 0094-243X. DOI: 10.1063/1.5138768. URL: https://aip.scitation.org/doi/abs/10.1063/1.5138768 (visited on 05/18/2021).

[18] Yuxing Liu, Marcello Canova, and Yue-Yun Wang. "Distributed Energy and Thermal Management of a 48-V Diesel Mild Hybrid Electric Vehicle With Electrically Heated Catalyst". *IEEE Transactions on Control Systems Technology* PP (June 2020), 1–14. DOI: 10.1109/TCST.2020.2997868.

[19] Michael Hopka, Devesh Upadhyay, and Michiel Nieuwstadt. "Smart DPF Regenerations - A Case Study of a Connected Powertrain Function". Apr. 2019. DOI: 10.4271/2019-01-0316.

[20] April Russell and William Epling. "Diesel Oxidation Catalysts". *Catalysis Reviews: Science and Engineering* 53 (Oct. 2011), 337–423. DOI: 10.1080/01614940.2011.596429.

[21] Feng Gao, Donghai Mei, Yilin Wang, János Szanyi, and Charles H. F. Peden. "Selective Catalytic Reduction over Cu/SSZ-13: Linking Homo- and Heterogeneous Catalysis". eng. *Journal of the American Chemical Society* 139.13 (Apr. 2017), 4935–4942. ISSN: 1520-5126. DOI: 10.1021/jacs.7b01128.

[22] J. Heywood. "Internal combustion engine fundamentals". 1988. DOI: 10.5860/choice.26-0943.

[23] *Commission Regulation (EU) 2017/1151 of 1 June 2017 supplementing Regulation (EC) No 715/2007 of the European Parliament and of the Council on type-approval of motor vehicles with respect to emissions from light passenger and commercial vehicles (Euro 5 and Euro 6) and on access to vehicle repair and maintenance information, amending Directive 2007/46/EC of the European Parliament and of the Council, Commission Regulation (EC) No 692/2008 and Commission Regulation (EU) No 1230/2012 and repealing Commission Regulation (EC) No 692/2008 (Text with EEA relevance)*. en. Legislative Body: GROW, COM. July 2017. URL: http://data.europa.eu/eli/reg/2017/1151/oj/eng (visited on 09/14/2021).

[24] Amy Lubeski. *Real-Time Catalytic Converter Temperature Estimator in the Powertrain Controller*. English. SAE Technical Paper 2000-01-0651. ISSN: 0148-7191, 2688-3627. Warrendale, PA: SAE International, Mar. 2000. DOI: 10.4271/2000-01-0651. URL: https://www.sae.org/publications/technical-papers/content/2000-01-0651/ (visited on 08/25/2021).

[25] P. J. Shayler, D. J. Hayden, and T. Ma. *Exhaust System Heat Transfer and Catalytic Converter Performance*. English. SAE Technical Paper 1999-01-0453. ISSN: 0148-7191, 2688-3627. Warrendale, PA: SAE International, Mar. 1999. DOI: 10.4271/1999-01-0453. URL: https://www.sae.org/publications/technical-papers/content/1999-01-0453/ (visited on 08/25/2021).

[26] Giuseppe Di Pierro. "Development of an integrated experimental and numerical methodology for the performance analysis of multiple hybrid electric architectures over different driving cycles". PhD thesis. Politecnico di Torino, 2020. URL: https://hdl.handle.net/11583/2843980.

[27] Alessandro Capancioni. "Development of a predictive thermal management function for Plug-in Hybrid Electric Vehicles". PhD thesis. URL: https://amslaurea.unibo.it/15248/.

[28] Mattia Boccolini. "Development of a speed profile prediction algorithm based on navigation data for energy management optimization". PhD thesis. URL: http://amslaurea.unibo.it/22543/.

[29] Tim Dallmann. "Costs of Emission Reduction Technologies for Diesel Engines Used in Non-Road Vehicles and Equipment". en (2018), 26. URL: https://theicct.org/sites/default/files/publications/Non_Road_Emission_Control_20180711.pdf.

[30] Stefan Pischinger, Joschka Schaub, Ferenc Aubeck, and Dieter van der Put. "Powertrain Concepts for Heavy-duty Applications to Meet 2030 CO2 Regulations". en. *ATZheavy duty worldwide* 13.3 (Sept. 2020), 36–41. ISSN: 2524-8774. DOI: 10.1007/s41321-020-0102-y. URL: https://doi.org/10.1007/s41321-020-0102-y (visited on 05/18/2021).

[31] Timothy Johnson and Ameya Joshi. "Review of Vehicle Engine Efficiency and Emissions". Mar. 2017. DOI: 10.4271/2017-01-0907.

[32] Zissis Samaras, S Hausberger, and Dr G Mellios. "Preliminary findings on possible Euro 7 emission limits for LD and HD vehicles". en (2020), 66. URL: https://circabc.europa.eu/sd/a/fdd70a2d-b50a-4d0b-a92a-e64d41d0e947/CLOVE%20test%20limits%20AGVES%202020-10-27%20final%20vs2.pdf.